2018

The Effects of Fire on Snow Accumulation, Snowmelt and Ground Thaw on a Peat Plateau in Subarctic Canada

Elyse Mathieu
math8590@mylaurier.ca

The Effects of Fire on Snow Accumulation, Snowmelt and Ground Thaw on a Peat Plateau in Subarctic Canada

By

Élyse Catherine Mathieu

BSc, University of Ottawa, 2014

THESIS

Submitted to the Department of Geography and Environmental Studies

In partial fulfillment of the requirements for

Master of Science in Geography

Wilfrid Laurier University

DEDICATION

A dedication to those most important in my life

To my family who has made me who I am today
You have been with me every step of the way through good time and bad
Thank you for the unconditional love, guidance and support you have given me

To my father who through thick and thin (and on short notice) has been there for me
You are the hidden strength behind my every success

To my loving mother who never failed to ask how my thesis was going and when I'll be done
Well mom here it is!

To my inspiring sister and the strongest person I know
For patiently putting up with me these past years

I love you to the moon and back

AUTHOR'S DECLARATION

I hereby declare that I am the sole author of this thesis. This is a true copy of the thesis including any required final revision, as accepted by my examiners. I understand that my thesis may be electronically available to the public.

DECLARATION OF CO-AUTHORSHIP

This thesis is a result of collaborative work with the co-authors listed in the manuscript. All co-authors provided expert advice and edits for the manuscript. Dr. Ryan Connon, Wilfrid Laurier University, provided support in conducting field measurements, advice on methodology and data analysis as well as overall support throughout the field seasons and writing process. Dr. Oliver Sonnentag, University of Montreal, provided instrumentation and expert advice on micrometeorological measurements and edits to the manuscript. Dr. William Quinton, Wilfrid Laurier University, provided financial support to conduct field work, support in the discussion of and an introduction to hydrological processes, as well as overall guidance on the project.

ABSTRACT

During the past century, the highest rates of warming have occurred at latitudes above 60^{o}N, where air temperatures have risen at twice the rate of other regions. In northwestern Canada, this warming has coincided with an increase in the frequency, size and severity of wildfires. The influence of such fires on the trajectory of on-going permafrost thaw is not well understood. As a consequence, the combined impacts of climate warming induced permafrost thaw and possible feedbacks arising from wildfires cannot be properly assessed. This study examines the impact of a 2.7 ha low-severity wildfire (July 2014) on water and energy flow processes that affect the timing and magnitude of ground thaw, including seasonal ground thaw, talik development and permafrost thaw. By comparing the end-of-winter snow water equivalent (SWE), rate of snowmelt and surface energy balance one year post-fire (2015) on an adjacent burned and unburned portions of a forested permafrost peat plateau as well as ground thaw and soil moisture three years post-fire (2015-2017).

Increase (16%) in snow depth had no significant direct impact on the increased rate and depth of ground thaw. Rather the increase in thaw depths resulted from a combination of factors: a longer thawing period due to an earlier (4 days) snowpack disappearance, an increase in energy available for snowmelt (36%) attributable to greater incoming shortwave radiation from the loss of radiative filtering provided by the canopy, decreased albedo and increased emitted longwave radiation from the charred trunks, contributing to the warmer soil temperatures at greater depths. Bulk thermal conductivity is lower in the burned forest soil as a result of drier soils. Thaw depths in the burned forest are significantly greater than thaw depths in the unburned forest, suggesting that the increased energy availability outweighs the impacts of a drier soil. Ground temperatures at 64 cm did not cool beyond the freezing point depression (-0.3°C), indicating an incomplete overwinter refreezing at this depth leading to the development of taliks.

Given the current warming trend in northwestern Canada, and that permafrost in this region is thin (< 10 m) and relatively warm (> -1°C), perturbation caused by a low-severity fire appears to be strong enough to induce talik development. In a peatland terrain underlain by discontinuous permafrost, talik development can sufficiently alter the thermal regime enough to trigger complete permafrost thaw. This study showed that a fire can change the amount of snow accumulation, the rate of its melt and disappearance, and the rate and pattern of ground thaw, which collectively alter key water flow and storage processes throughout the burned area.

KEY WORDS: fire, hydrology, snow, energy balance, active layer, permafrost, talik, peat plateau

ACKNOWLEDGEMENTS

First and foremost, I would like to thank my master's supervisor, Dr. Quinton, for believing in me from the beginning of this long process all the way to the end. Your advice and knowledge has been invaluable. I would not be here today without your support.

I would like to thank the many experts who provided support throughout my thesis. Dr. Aaron Berg and Dr. Oliver Sonnentag, as well as their students, who helped during the field seasons with data collection and afterwards providing aid and advice on analysis. Dr. Phil Marsh and Dr. Brent Wolfe for participating in my thesis defense. A big thank you to Dr. Jason Venkiteswaren, who repeatedly gave me the opportunity as his TA. Without your kind words of support and opportunity to teach young minds I don't believe I could have enjoyed my time as much at Wilfrid Laurier University.

I would also like to sincerely thank all of the graduate students and research assistants who helped with the data collection and made the many months spent on the field and unforgettable experience. Thank you very much: Caren Ackley, Ryan Connon, Elise Devoie, Jessica Hanish, Manuel Helbig, Karolyn Kirsch, Jared Simpson, Lindsay Stone, and Becca Warren. A very special thanks to Emily Haughton, who laid down the stepping stone for snowmelt energy balance modelling.

Finally I would like to thank all of my family and friends for sticking with me through thick and thin these past years. It's been an adventure of ups and downs, but I could not have done it without the support from each and everyone one of you!

TABLE OF CONTENTS

LIST OF TABLES

LIST OF FIGURES

CHAPTER 1

1 – INTRODUCTION

The following thesis has been organized into three distinct chapters. The first chapter includes a literature review of relevant research previously conducted on forest fires, studies from the Scotty Creek basin, as well as a summary of objectives and methods of the research conducted. The following chapter focuses on presenting the major findings of the research. The final chapter summarizes the principle findings and future potential work.

1.1 – Literature Review

In the northern hemisphere, air temperatures have increased during the last half century throughout much of the circumpolar region (IPCC, 2014). During this same period, the temperatures of permafrost have increased following the rise in mean annual air temperatures in Alaska, Canada, and Russia (Vitt *et al*., 2000). Permafrost is defined as soils whose temperatures persist continuously at or below 0°C for a minimum of two consecutive years (Muller, 1947). Northwestern Canada is among the most rapidly warming regions on Earth (Ji *et al*., 2014). The permafrost of this region is relatively thin and warm and, as such, is highly susceptible to thaw (Beilman and Robinson, 2003). In the region of thawing discontinuous and sporadic permafrost (10 to < 50% of the land surface underlain by permafrost), a majority of the landscape is dominated by peatlands (Chasmer *et al*., 2011).

Peatlands are ecosystems with cold soils where the net primary productivity exceeds decomposition rates, resulting in the accumulation of thick organic deposits. Peat plateaus are permafrost-cored peatlands, elevated above the surrounding wetlands due to the volumetric expansion of ice. Peat plateau's are the dominant land cover type underlain by permafrost in low-

relief sporadic discontinuous permafrost terrains. Peat plateaus are typically vegetated with a black spruce (*Picea mariana*) forest cover (Beilman and Robinson, 2003). The presence of trees allows for more effective snow interception and reduces solar radiation (Vitt *et al*., 2000), which serve to insulate the underlying permafrost. Climate warming induced permafrost thaw often co-occurs within permafrost thawing areas affected by other disturbances, such as forest cover removal during seismic exploration (Williams and Quinton, 2013), logging operations (Fedorov *et al*., 2017), or wildfires (Smith *et al*., 2015; Helbig *et al*., 2016).

Wildfires are a natural part of the boreal forest where 1 million hectares (ha) are burned each year, however the intensity and frequency of wildfires has tripled in the last half century (Stocks *et al.*, 2003; Yoshikawa *et al.*, 2002; Wang *et al*., 2015). Since 1990, approximately 17 365 100 ha has been subject to burning in the NWT, representing approximately 81% of the forested area in the territory (National Forestry Database, 2016). Furthermore, the frequency and size of fires are expected to continue to increase over the coming decades (Flannigan *et al*., 2005, 2013; Wotton *et al.*, 2010). Despite the large areal footprint of wildfires and its projected growth, very little is known about how fires affect permafrost and the key processes that affect the cycling and storage of water on permafrost landscape. The severity of wildfires may have an influence on the extent to which it can affect hydrological processes. For example, a severe fire removes the tree canopy, the sub-canopy, and the upper organic soil horizons, while a minor fire may only remove tree needles, small branches, and blacken the ground surface without removing organic layers.

A forest canopy plays an important role in snow hydrology, affecting snow accumulation and melt as well as surface and subsurface thermal regimes. The canopy reduces the amount of short-wave radiation reaching the snow or ground surface, increases emitted long-wave radiation,

and attenuates the exchange of latent and sensible heat through the reduction of wind speed, near-surface temperatures, and humidity gradients. Removal of the forest canopy exposes the snow or ground surface to greater incident solar radiation and higher wind speeds, which can increase sensible and latent heat inputs (Winkler *et al.*, 2010).

Fires influence both forest structure and function (Soja *et al.*, 2006). Wildfires open forest canopies, altering end of winter snow conditions and hydrological processes such as snowmelt and ground thaw (Brown *et al*., 2015). Although wildfire disturbances are extensive, the impacts on snow accumulation and snowmelt patterns as well as ground thaw rates are still poorly understood and rarely considered in hydrological models.

1.1.1 – Snow Accumulation and Snowmelt

Snow accumulation varies depending on the topography, vegetation, and meteorology of the region (Andreadis *et al.*, 2009). The canopy of a boreal forest can intercept up to 60% of annual snowfall. Of this intercepted snow, 30% can return to the atmosphere as vapor through sublimation (Pomeroy and Schmidt, 1993). The remaining 70% of intercepted snow can be re-suspended, redistributed, or unloaded to the forest snowpack. A fire which partially or completely removes the tree canopy will disrupt the snow interception, sublimation, and accumulation processes (Winkler, 2011), subsequently, altering snowmelt via increased solar inputs.

A fire can remove up to 90% of the forest cover (Woods *et al.*, 2006), a process which dramatically reduces the interception of snow and rainfall, and therefore increases the amount of precipitation reaching the ground (Winkler *et al.*, 2010). In southern NWT, ~50% of the total annual precipitation falls as snow (MSC, 2016), which upon melt is the dominant hydrological

event of the year in sub-arctic nival basins. As a result, the snow water equivalent (SWE) in a burned coniferous forest can increase by 10 to 50% compared to a forested stand (Woods *et al.*, 2006; Winkler, 2011) because of the reduction in the interception efficiency of the tree canopy following a burn (Burles and Boon, 2011).

Just as the canopy acts as a filter for snow, it is also responsible for reducing the solar irradiance reaching sub-canopy vegetation and the ground surface of a forest. Prior to a burn, the daily total incoming shortwave radiation (K↓) penetrating the canopy and reaching the ground surface is typically lesser than the amount arriving at the top of the canopy (Chambers *et al.*, 2005). Following a fire, the daily total K↓ reaching the ground surface is greater compared to pre-fire conditions (Kasischke *et al.*, 1995). Considering that K↓ is the greatest contributor to the energy consumed for snowmelt (Q_m) (Chambers *et al.*, 2005; Burles and Boon, 2011) a burn has the potential to greatly alter snowmelt rates and patterns.

A greater input of energy for snowmelt can result in a significantly higher ablation rate in a disturbed forest. Ablation refers to the loss or disappearance of a snowpack caused by snowmelt, evaporation and sublimation. Vapour losses as evaporation and sublimation are minor relative to the rates of snowmelt (Bernier and Swanson, 1992; Winkler *et al.*, 2010). Previous studies have found the average snow ablation rates can increase from 38 to 57% in a burned forest (Woods *et al.*, 2006; Redding *et al.*, 2007). The increased input of solar energy to a burned forest can decrease the duration of the snowmelt period by several days (Burles and Boon, 2011). For example, a 30% increase in available snowmelt energy decreased the snowmelt period by six days in a burned forest (Boon, 2009; Winkler, 2011). As a snowpack insulates the underlying ground surface, where ground surface temperatures can remain relatively warm under a thicker snowpack and are cooler under thinner snowpack (Jungqvist *et al.*, 2014).

1.1.2 – Ground Thaw

The active layer (AL) is the layer of ground above permafrost that thaws and freezes annually (Muller, 1947). The energy flux that thaws and refreezes the AL is transferred primarily by thermal conduction to and from the ground surface (Woo, 2012). The energy flux into the ground is driven by the thermal gradient between the ground surface and the upper surface of the frozen layer of ground, divided by the distance separating them. During the ground thaw season, the upper surface of the frozen layer, often referred to as the frost table (FT), is assumed to maintain a temperature close to 0°C. As the distance to the FT increases with time over the thaw season, the thermal flux into the ground and the rate of ground thaw decrease.

The net energy at the ground surface (Q*) available to drive surface-atmosphere exchange is strongly influenced by albedo and surface temperature (Chambers *et al.*, 2005; Rouse and Mills, 1977). A common feature shared by spruce canopies is a low albedo of ~0.10, formed mainly as a result of efficient radiation trapping (Stenberg *et al.*, 1995). Following wildfires, the surface albedo is significantly decreased, to as much as 0.05, depending on the extent of the burning (Yoshikawa *et al.*, 2002; Chambers *et al.*, 2005). Large reductions of ground surface albedo in response to wildfires have been documented for black spruce forests, even for relatively light burns (Yoshikawa *et al.*, 2002; Chambers *et al.*, 2005), which is due to the charring of the surface and the increased transmissivity of shortwave radiation. Increased sensible heat flux (Q_h), converted from K↓, contributes to surface heating, which in turn results in higher ground surface temperatures (Chambers *et al.*, 2005; Liu *et al.*, 2014; Yoshikawa *et al.*, 2002; Zhang *et al.*, 2015). Increases in ground surface temperatures thereby increase the downward directed thermal gradient and thermal flux conducted into the ground at greater depths (Table 1).

Wildfires also affect the ground refreezing process. For example, Pomeroy *et al*. (2012) demonstrated that fire reduces the snow interception efficiency of a black spruce canopy. As a result, snow on the ground accumulates to greater depths, and the ground is more thermally insulated. Refreezing of the ground takes longer and does not penetrate to as great a depth as it would under an otherwise thinner snowpack. This process suggests a delayed refreezing of the ground below a burned canopy, although it may be offset by greater radiative cooling of a snowpack below a burned tree canopy. Longwave down-welling to the snowpack surface from such a canopy would be less than that from an unburned forest, given the far greater surface area of the latter. The enhanced radiative cooling of a snowpack beneath a burned tree canopy can be augmented by enhanced ventilation due to increased wind turbulence over the snowpack surface (Lau *et al*., 2010).

Typically, seasonal ground thawing ceases by late August or early September in the southern NWT (Wright *et al.*, 2009). In a warming climate, thaw depth during summer eventually exceeds the depth of refreeze, giving rise to a perennially thawed layer (*i.e.* talik) separating the AL from the underlying permafrost (Neuendorf *et al*., 2005). The layer above the permafrost is called the suprapermafrost layer and is comprised of the AL and, if present, a talik (Muller, 1947; Connon *et al.*, 2018).

A wildfire may not always affect the underlying permafrost, and as such is dependent on the severity of the burn (Table 1). Thickness of the AL is strongly controlled by the thickness of the overlying organic layer, and the thermal conductivity and moisture content of the entire soil profile (Shur and Jorgenson, 2007; Yoshikawa *et al.*, 2002). The thickness of the organic layer that persists following a fire can be an important control on the fate of the underlying permafrost. Increased suprapermafrost layer thickness (SLT) tends to develop in burns with greater loss of

organic matter (Mackay, 1970; Brown, 1983). The effect of fire on the SLT has increased since 1990 due to climate warming in Central Alaska (Kasischke *et al.*, 2007). The removal of sun-shading tree canopies and insulating peat layers as well as the charring of the ground surface by fire results in changes to ground surface energy exchange as represented by the increased SLT.

1.2 – Objectives

In the southern Taiga Plains, climate warming has led to increased rates of permafrost thaw involving both extensive talik development and suprapermafrost layer thickening (Connon *et al*., 2018). This study aims to evaluate wildfire effects on a peat plateau in the discontinuous permafrost zone. The effects of a low-severity wildfire on the rate of snowmelt and subsequent ground thaw are quantified and compared to an adjacent unburned plateau to better characterize post-fire differences for hydrological modeling of snow-dominated watersheds. This study seeks to build an integrated understanding of how wildfires affect active layer hydrological processes by examining:

i) the relative impact on overwinter permafrost energetics from the increased insulation of a thicker snowpack in conjunction with enhanced radiative cooling beneath a burned (and more open) tree canopy;

ii) the relative importance of increased net shortwave radiation resulting from a lower albedo and a decreased bulk thermal conductivity due to drier soil conditions; and

iii) if taliks develop from a low-severity burn, and if so, are they transient features that disappear as the ground surface is re-vegetated, or do they persist.

1.3 – Methods

This subsection is an overview of the data collected and methods of analysis.
For further details refer to Chapter 2, section 2.4 Methods

A recently (2014) burned peat plateau and adjacent unburned portion was instrumented in order to conduct a detailed analysis of above and below ground energy balance to quantify the effects of a low-severity fire on permafrost degradation in hydrological models. The burned plateau in question, is located east of Goose Lake (Figure 1) in the Scotty Creek watershed, 50 km south of Fort Simpson, Northwest Territories, Canada. An intensive field survey was conducted along a 150 m west to east transect during the winter and spring of 2015. While other measurements we're taken at 5m intervals in a grid (50 x 50 m) installed in both burned and unburned portions was sampled once a year in August 3 years post-fire (2015-2017). The field survey was designed to collect data on winter snow accumulation and melt rates from March to June, as well as subsequent ground thaw at the beginning of the season (June) and end of summer in August.

Winter field measurements collected snow depth (cm) and density (g cm^{-3}) from a combination of snow pits and snow surveys measured along the transect, as well as ablation (mm day^{-1}) at several points in both the burned and unburned portions of the peat plateau. An unmanned aerial vehicle (UAV) imagery was acquired over the field season used to determine the snow covered area (SCA) during snowmelt when the site was inaccessible due to unstable ice conditions during breakup.

Instrumented tripods were used to quantify the differences in meteorological conditions on the two portions of the plateau. Meteorological data was used in a process-based snowmelt model following an energy balance approach (Burles, 2010; Boon, 2009) to calculate the energy available

for snowmelt and simulate melting of the snowpack (Haughton, 2018). Variables were parameterized from field snowpack measurements and literature values (see Supplementary Materials). The output was validated with snow water equivalent (SWE; mm) measured from field snow surveys. The computed depth of the snowpack in the unburned forested area correlated with the observed average snow depth and showed no significant difference ($p < 0.05$), as such was used as a proxy in calculating the energy available to melt the snowpack (Q_m).

The summer field measurements collected from transect surveys included depths to the frost table (FT) and the characterization of the ground cover vegetation at each measurement point one year (2015) post-fire. Absolute elevation of each FT measurement was acquired by DGPS. Frost table depth as well as paired integrated 20 cm soil moisture (%) measurements were taken 3 years post-fire in the burned and unburned plateau at the grid locations to be used in a multi-year analysis of talik development.

Measured FT depth from the grid survey three years post-fire (2015-2017), was used as a measurement the suprapermafrost layer thickness (SLT) annually. The purpose of these grids is to track changes in thaw depth and soil moisture between the two sites over time. Increases in the SLT greater than the maximum depth of overwinter refreeze (0.8 m; Connon *et al.*, 2018) is the threshold indicator for talik development.

Statistical analysis' of the burned to unburned portion of the plateau allowed for a comparison and identification of significant changes with low-severity fires to the hydrological cycle. A conceptual model was developed to illustrate the interlinked effects of wildfire during the snowmelt process and the ground thaw season leading to permafrost degradation.

CHAPTER 2

The impact of a low-severity burn on the trajectory of permafrost thaw: Scotty Creek, Northwest Territories, Canada

É.C. Mathieu[1*], R.F. Connon[1], O. Sonnentag[2], W.L. Quinton[1]

[1]Cold Regions Research Centre, Wilfrid Laurier University, Waterloo, Canada, N2L 3C5

[2]Department of Geography, University of Montreal, Montreal, Canada, Montréal, H2V 2B8

2.1 – INTRODUCTION

The southern Taiga Plains ecoregion in northwestern Canada is one of the most rapidly warming regions on Earth (Ji *et al*., 2014). This region is dominated by peatlands in the form of forested peat plateaus underlain by permafrost, and treeless, permafrost-free wetlands including channel fens and collapse-scar bogs (Quinton *et al.*, 2003). In this region sporadic discontinuous permafrost (*i.e.* 10 to 50% of the land surface overlies permafrost), is relatively thin (5-15 m) and warm (*i.e.* at or near 0°C). As such it is highly susceptible to thaw (Beilman and Robinson, 2003; Helbig *et al*., 2016).

Recent studies in the southern Taiga Plains have documented increasing rates of permafrost thaw with resulting transformations of forested permafrost plateaus to permafrost free and treeless wetlands (Chasmer and Hopkinson, 2016), with the thaw process driven mainly by lateral heat convection from the adjoining saturated environments (Kurylyk *et al*., 2016). Vertical heat flux thickens the suprapermafrost layer through heat conduction at the ground surface, this process is

* Corresponding Author. Email: Elyse.C.Mathieu@gmail.com

just as important as lateral thaw. Thaw rates have been shown to be accelerated by disturbances such as tree die-off (Baltzer *et al*., 2014), linear disturbances such as seismic lines (Williams *et al*., 2013) and wildfire (Smith *et al*., 2015). Energy flows downward through the active layer primarily by conduction driven by the thermal gradient between the ground surface and the upper surface of the frozen layer of ground (Hayashi *et al*., 2007). During seasonal soil thawing, the upper surface of the frozen layer, often referred to as the frost table (FT), maintains a temperature close to 0°C as it lowers through the profile. As the depth to the FT increases with time over the thaw season the thermal energy received at the FT decreases and as a result so too does the rate of ground thaw.

Typically, seasonal ground thawing ceases by late August or early September in the southern Taiga Plains (Wright *et al.*, 2009). The layer of ground above permafrost that thaws and freezes annually is by definition the active layer (Muller, 1947). In discontinuous permafrost terrain a warming climate increases thaw depths during summer which eventually exceeds the depth of refreeze, giving rise to a perennially thawed layer (*i.e.* talik) separating the active layer from the underlying permafrost (Neuendorf *et al*., 2005). The layer above the permafrost (*i.e.* suprapermafrost layer) is comprised of the active layer and talik. In the southern Taiga Plains, climate warming has led to increased permafrost thaw involving both extensive talik development and suprapermafrost layer thickening (Connon *et al*., 2018).

Wildfires are a natural process of the boreal biome, with approximately one million hectares burned annually throughout the circumpolar region (Bernhardt *et al*., 2011). However, climate warming appears to be changing forest fire regimes (Wotton *et al.*, 2010). Several studies have reported significant increases in the intensity and frequency of wildfires in the boreal region during the past half century (*e.g.* Flannigan *et al*., 2013; Stocks *et al.*, 2003; Yoshikawa *et al.*, 2002; Wang *et al*., 2015). The geographic area affected by fires also appears to be increasing. For

example, over 16 million ha of the Northwest Territories (NWT) burned between 1990 and 2015 (National Forestry Database, 2016), more than double the total from the previous 25 years (1965-1990) (Stocks *et al*., 2003). Increases in fire frequency, intensity and areal extent are expected to continue during the coming decades (Flannigan *et al*., 2005; Wotton *et al.*, 2010).

It has been demonstrated that forest fires can initiate permafrost thaw (Smith *et al*., 2015), but in certain conditions after a period of years to decades, the permafrost returns its pre-burn condition (Jafarov *et al*., 2013). However, there is little understanding of the impact of wildfire on the permafrost in environments where permafrost thaw has already been initiated by a warming climate, although the literature provides some key insights (Zhang *et al*., 2015). For example, large reductions of ground surface albedo in response to wildfires have been documented for black spruce forests, even for relatively light burns (Yoshikawa *et al.*, 2002; Chambers *et al.*, 2005), due to the charring of the surface and the increased absorption of incoming solar radiation. This albedo reduction increases the ground surface temperature thereby increasing the downward directed thermal gradient and thermal flux conducted into the ground (Chambers *et al*., 2005).

Boreal forest tree canopies filter moisture and energy flows between the atmosphere and the ground surface. As such, changes to the tree canopy resulting from a burn can affect the accumulation, re-distribution, and melt patterns of snow on the ground, and subsequently, the energy regime of the suprapermafrost layer. During winter, the snow covering the ground provides thermal insulation for the underlying permafrost, with the degree of insulation increasing with snow depth (Smith *et al*., 2015). Dense boreal forest canopies can intercept as much as 60% of total annual snowfall (Pomeroy and Gray, 1995; Andreadis *et al.*, 2009), of which 30% can return to the atmosphere as water vapour through sublimation (Pomeroy and Gray, 1995; Pomeroy and Schmidt, 1993). The remaining 70% is re-suspended, redistributed or unloaded to the snowpack

on the ground. Partial or complete removal of the tree canopy by fire can increase the depth of snow on the ground by reducing both canopy interception and subsequent sublimation. This increase is most pronounced for severe fires since they can remove up to 90% of the forest cover (Woods *et al.*, 2006). Following a burn, the snow water equivalent (SWE) was found to increase by 45% in the southern boreal forest (Pomeroy *et al*., 2012), and by over 50% in the subalpine boreal forest (Burles and Boon, 2011; Table 2).

For a healthy black spruce forest in the southern boreal, only 25 to 35% of the daily total incoming solar radiation (K↓) arriving at the top of the canopy is transmitted to the forest floor. Following a burn, this can increase by 60 to 90% (Chambers *et al*., 2005; Kasischke *et al*., 1995). At Scotty Creek, in the southern NWT, a dense black spruce forest cover transmits 50-60% of the total daily top of canopy K↓ to the forest floor, while an adjacent sparse forest transmits approximately 80% (Connon *et al*., 2018). Since the majority of energy for snowmelt (Q_m) is supplied by K↓ (Chambers *et al.*, 2005; Burles and Boon, 2011), the volume and timing of snowmelt water delivery to the ground is expected to change following a burn. For example, the daily snowmelt rate was found to be 57% higher in a burned boreal forest stand than an adjacent unburned stand (Skidmore *et al.*, 1994; Winkler, 2011). For increasing burn severity, reported snowmelt rates have been found to increase (Burles and Boon, 2011), and snowmelt period duration has been shown to decrease (Winkler, 2011). These field observations were supported by numerical simulations that indicate a 10-35% increase in snowmelt rate can reduce the snowmelt period by seven days in a burned forest (Spittlehouse, 2008; Table 2). Given that spatial variation in soil moisture content is the primary factor controlling spatial variations in the rate of ground thaw at peatland-dominated sites in the southern Taiga Plains (Hayashi *et al.*, 2007; Williams and

Quinton, 2013), such burn-induced changes to the timing and volume of snowmelt water delivery to the ground has the potential to alter the moisture and therefore the thermal regimes of the ground.

Despite the large and growing footprint of wildfires in the southern Taiga Plains, a region of widespread permafrost thaw, the current understanding of how wildfires affect the trajectory of this thaw is poor. In large part this is due to the lack of clarity of the net impact of the numerous, well documented burn-induced changes to mass and energy flow processes, including possible feedback processes. Some examples of potential feedback processes requiring further study include (i) the extent to which the increased insulation of the permafrost resulting from greater depth of snow on the ground may be offset by greater radiative cooling of a snowpack below a burned tree canopy; (ii) the extent to which enhanced radiative cooling of a snowpack beneath a burned tree canopy is augmented by enhanced ventilation due to increased wind turbulence over the snowpack surface resulting from the lower aerodynamic roughness of a burned canopy; (iii) the relative impact on permafrost of the increased mass (snow) resulting in greater thermal insulation of the ground, and of increased transmissivity ($K\downarrow$) leading to greater energy availability to snowmelt (Q_m) and ground thaw (Q_g). Following the removal of the snow cover, the lower albedo of the ground surface at a burned site enables greater energy availability at the ground surface, resulting in greater thaw rates than at unburned sites. However, iv) drier near-surface soils (and therefore less thermally conductive) potentially offsets the burned site lower ground surface albedo reducing the net effect on the ground heat flux at a burned site is not well understood (Kasischke *et al*., 2007; Kopp *et al*., 2014). There is also v) a lack of understanding on the relative importance of the increased availability of energy for ground thaw (due to greater canopy transmissivity of radiation and reduced ground surface albedo), and the decreased moisture content and therefore reduced thermal conductivity of the upper soil layers (due to increased radiative and

aerodynamic energy available for evapotranspiration). The former is a thaw-inducing process whereas the latter reduces ground thaw. As explained above, if the loss of energy from the ground during winter is insufficient to completely refreeze this thicker layer of thawed ground, a talik will form. The process of burn-induced talik development is well-documented for high-severity burns (Brown *et al.*, 2015; Smith *et al.*, 2015; Yoshikawa *et al.*, 2002), but vi) it is not clear if this would also occur for a low-severity burn, and if such burn induced taliks are transient features that disappear as the tree canopy and ground surface is re-vegetated, or if they persist. Improving the understanding of these burn-induced changes to mass and energy flow processes, including possible feedback processes is an important step toward predicting how such burns might affect the trajectory of on-going permafrost thaw.

Objectives:

This study seeks to build an integrated understanding of how wildfires affect active layer hydrological processes by examining: i) the relative impact on overwinter permafrost energetics from the increased insulation of a thicker snowpack in conjunction with the assumption of enhanced radiative cooling beneath a burned (and more open) tree canopy; ii) the relative importance of increased net shortwave radiation resulting from a lower albedo and a decreased bulk thermal conductivity due to drier soil conditions; and iii) if taliks develop from a low-severity burn, and if so, are they transient features that disappear as the ground surface is re-vegetated, or do they persist, continuously degrading the underlying permafrost.

2.2 – STUDY SITE

This study is focused on a single peat plateau in the headwater area of Scotty Creek (61°17’83"N, 121°17’25"W) in the sporadic permafrost zone of the southern Northwest Territories (NWT), Canada (Figure 1a). The region is characterized by a dry continental climate, short, dry summers and long, cold winters. Average (1981-2010) annual air temperature (T_{air}) is -2.8°C and average annual precipitation is 388 mm (Figure 2a), 48% of which is snow (MSC, 2016). Mean T_{air} in northwestern Canada has increased in winter months by as much as 6°C from 1948-2012 (Vincent *et al*., 2015). Total annual precipitation in the same region has significantly increased during the past 65 years (Vincent *et al*., 2015; Zhang *et al.*, 2015). Snowfall to rainfall ratio has remained relatively constant in the area over the same time period. In the Scotty Creek basin, snowmelt typically commences early April, such that by May only small amounts of snow remain on the ground.

The major land cover types characterizing the Scotty Creek headwaters include forested permafrost plateaus (hereafter "peat plateaus") and permafrost-free wetlands dominated by channel fens and collapse-scar bogs (Figure 1c). The vegetation of the study plateau is typical of the peat plateaus at Scotty Creek and consists of a black spruce (*Picea mariana*) dominated overstory, an understory of birch shrubs (*Betula spp.*) and a ground cover of Labrador tea (*Rhododendron groenlandicum*), lichen (*Cladina mitis*), feather moss (*Pleurozium schreberi*) and *Sphagnum* sp. mounds on relatively dry peat (Williams *et al*., 2013). Peat plateaus in southwestern NWT consist of an organic layer of varying thickness (0.5-8 m), overlying a glacial till of silt-clay sized particles of low permeability (McClymont *et al.*, 2013). The average tree height is 2.2 m and stand density is 0.12 stems m^{-2} with an overstory leaf area index (LAI; LAI-2200 Plant Canopy Analyzer, Li-COR Biosciences, Lincoln, NE, USA) estimated at Scotty (Sonnentag *et al.*, 2007)

in 2015 of 0.74 ± 0.33 m^2 m^{-2} and a bog LAI measurement of 0.47 ± 0.40 m^2 m^{-2}. The study plateau rises 1.2 m above the surrounding wetland. Although direct measurements of permafrost thickness were not made at the study plateau, geophysical investigations by McClymont *et al.* (2013) determined that permafrost thicknesses at several neighbouring plateaus ranges between 5 and 13 m.

In July 2014, a year with the highest recorded total forested area burned (3 416 291 ha) in the NWT (National Forestry Database, 2016), a relatively small fire (2.7 ha) burned a portion of a peat plateau (hereafter "burned plateau") on the southeast side of Goose Lake (Figure 1b). The fire removed the foliage from the tree canopy and the understory, leaving charred black spruce trunks and larger branches still intact. The ground surface was unevenly burned with surfaces at higher elevations (*i.e.* hummocks) more deeply burned than hollows. By the end of the growing season in August 2015, Labrador tea had re-colonized much of the burned area, although to a lesser extent than the pre-burn cover of this species as indicated by the Labrador tea cover at the adjacent unburned portion of the peat plateau (hereafter "unburned plateau").

2015 was a relatively warm and dry year compared to the 30 year (1981 to 2010) climate monthly normals (Figure 2). During the study period from March to August 2015, monthly average T_{air} (Table 3) was warmer (8.4℃) than normals (7.1℃). Approximately 56% (188 mm) of the total (*i.e.* rain and snow) annual precipitation for 2015 fell during the March to August study period. This is slightly less than the average value of 61% (236 mm) for the 30-year period referred to above. In 2015, there was substantially less precipitation in May (69.4% decrease) and June (77.2% decrease) compared to the 30 year monthly normal (Table 3).

2.3 – METHODS

Micrometeorological measurements we're taken continuously three years following the fire of July 2014, on a burned portion and adjacent unburned portion of the study peat plateau. Intensive field measurements were made in the first year (2015) post-fire to evaluate the impacts of fire on late-winter snow accumulation, snowmelt, and seasonal ground thaw progression. While the suprapermafrost layer thickness (SLT) and soil moisture measurements were taken three years post-fire (2015 and 2017), to identify talik development due to a low-severity fire leading to the degradation of the permafrost.

2.3.1 – Micrometeorological Measurements

Two meteorological stations (Figure 3) were installed in August 2014, one in the burned and the other in the unburned portion of the study plateau, approximately one month after the fire. Using identical instrumentation on both tripods, four component radiation (K↓, K↑, L↓, L↑, W m^{-2}) (CNR4, Kipp and Zonen, Delft, Netherlands), and air temperature (T_{air}, °C; HC-S3-XT Rotronic Instrument Corp., Bassersdorf, Switzerland), wind speed and direction (μ; RM Young, Traverse City, MI, USA), were measured within the canopy at two meters above the mean ground surface and snow depth (SR50A, Campbell Scientific, Logan, UT, USA) at 1.4 m above the ground surface. Soil temperature (T_{soil}, °C) was measured in close proximity to both tripods along vertical profiles at 2, 4, 8, 16, 32 and 64 cm below the ground surface using type "T" thermocouple wires (Omega Engineering, Stamford, CT, USA). Snow temperatures were measured using the same approach at 10, 20 and 30 cm above the ground surface.

2.3.2 – Field Survey Measurements

Snow depth and density measurements (Geoscientific snow tube and scale; 6.18 cm diameter) began on 30 March 2015, and were conducted along a 150 m study transect (Figure 1c) every second day to estimate snow water equivalent (SWE) during the snowmelt period. Snowmelt rates were measured with ablation strings until 27 April. On-site measurements resumed on 10 May once the lake could be safely crossed by canoe. From this date onwards until 26 June, thaw depths were measured using a two meter graduated steel frost table (FT) probe along the same study transect as snow surveys bi-weekly, and at end of season on 25 August 2015. The depth of the FT measurements taken at the end of August 3 years post-fire (2015-2017), also known as the suprapermafrost layer thickness (SLT), encompassing the active layer as well as underlying taliks above the permafrost table. The SLT in August was assumed to be representative of the maximum extent of seasonal thaw and the location of the permafrost table, given that the maximum thaw depth occurs approximately two weeks prior to the start of soil refreezing (Wright *et al*., 2009). All measurement points were geo-located using differential GPS (Leica GS10 RTK GPS, Heerburg, Switzerland; Hz 8 mm + 1 ppm/ V 15 mm + 1 ppm). At each thaw depth measurement, location the above ground vegetation was identified and the measurement point was classified as lichen, moss (*Sphagnum* sp.), or charred surface to evaluate the effect of ground cover on the seasonal thaw depths. With each FT depth measurement within the grid, a paired 20 cm depth integrated soil moisture (%; Hydrosense, Campbell Scientific) measurement was taken as well.

2.3.3 – Aerial Remote Sensing

An unmanned aerial vehicle (UAV, Phantom 2+ Vision; DJI, Shenzhen, China) was used to acquire aerial remote sensing images of the burned and unburned forest sites daily from 10 April

to 12 May 2015, to document the change in snow covered area. This platform is designed for aerial photography and has a lightweight, multi-functional camera (14 Megapixel, 4384 x 3288) on a 3-axis stabilizing gimbal. Image resolution (ground pixel diameter), at a constant flying height of 30 m above the ground is approximately one cm. Using DJI PC ground station software, a flight path over study transect was pre-programmed, and flown bi-daily at a velocity of five m s^{-1}. Stills were then corrected for the distortion resulting from the fish eye lens on the camera (Adobe Photoshop Lightroom 5.7; San Jose, CA, USA), orthorectified, and mosaiked into transect images (Figure 3). UAV imagery was employed in this study as a means of calculating the snow cover depletion during snowmelt and as a method of assessing snowmelt rates when the study site was inaccessible. Daily images of the transect were analyzed with ImageJ (https://imagej.nih.gov/ij/), using 8-bit binary images which enable the measurement of snow covered and snow-free pixels to calculate the percentage of snow covered area. The earliest imagery acquired on 10 April was used as a standard to correct for the percentage of trees, which are perceived as snow-free pixels. A snow cover depletion curve can infer the loss of snow mass from a regression of the snow covered area (SCA) and measured SWE on the landscape throughout the snowmelt season during the period when the site could not be accessed for several days.

2.3.4 – Snowmelt Energy Balance

The energy available for snowmelt Q_m is governed by the energy balance defined as:

$$Q_m = K^* + L^* + Q_e + Q_h + Q_g + Q_r - Q_{cc} \quad (1)$$

where K* and L* are the net shortwave and net longwave radiation components, respectively, Q_e and Q_h are calculated latent and sensible heat fluxes, respectively. The ground heat flux (Q_g) was

calculated (see supplemental materials) and deemed negligible at this site. Q_r the heat flux input from rain was omitted from calculations as there was no rainfall events during the snowmelt period of 2015. The cold content (Q_{cc}) is the energy required to raise the temperature of the snowpack to the melting point. Net radiation (Q*) was calculated from the sum of the K* and L*, which were directly measured from the four-component radiometer on both the burned and unburned portions. All units are W m^{-2}, summed from hourly measurements and converted to MJ m^{-2} day.

The Q_e and Q_h were computed using the bulk aerodynamic method (Andreas, 2002). The Q_e and Q_h are the exchange of energy from the snow surface and the overlying air mass due to the gradient of T_{air} or vapor pressure, respectively (Boon, 2009). Under neutral atmospheric conditions, the bulk transfer coefficient for sensible heat equals the bulk transfer coefficient for latent heat (Burles, 2010) and can be derived from the bulk transfer coefficient for momentum (Price and Dunne, 1976). Over melting snow, the snow surface is 0°C, the T_{air} is above 0°C, resulting in atmospheric stability (Price and Dunne, 1976). The cooler, denser air above the snowpack remains stable with atmospheric turbulence and reduces the rates of turbulent fluxes (Boon, 2009). Atmospheric conditions over the snow surface can also become unstable, a condition more uncommon however not impossible (de la Casinière, 1974). The aerodynamic method (Richardson number; Ri) used at other boreal regions (*e.g.* Price and Dunne, 1976; Andreas, 2002; Boon, 2009; Burles, 2010) was used to correct the bulk transfer coefficients used in the calculation of the turbulent fluxes which are essential to computing Q_m. The Richardson bulk stability parameter (Ri; dimensionless) is used to assess the stable ($Ri > 0.3$) and unstable ($Ri < 0.3$) atmospheric conditions (Andreas, 2002), to properly calculate a corrected bulk transfer coefficient under stable and unstable conditions (Price and Dunne 1976; Monteith, 1957). The cold content was computed from snow temperature measurements as:

$$Q_{cc} = -c_i * \rho_w * SWE * (T_s - T_m) \quad (2)$$

where c_i is the heat capacity of ice (2102 J kg^{-1} K^{-1}), ρ_w is the density of water (1000 kg m^{-3}), SWE the snow water equivalent (mm), T_s is the average snowpack temperature (℃), and T_m is the melting point temperature (0℃) (Dingman, 2002). As the surface of the melting snowpack lowered, only the thermistors still within the snow were used for the calculation, as it would otherwise be measuring air temperature instead of internal snowpack temperature.

The computed snowmelt rates (M; mm) are calculated on an hourly time step from Q_m:

$$M = {Q_m}/{L_f * \rho_w} \quad (3)$$

where L_f is the latent heat of fusion (334 J g^{-1}). Equation (3) was validated by comparison to measured daily melt rates. Measured melt was calculated two ways, from the ablation string measurements and from the SWE point calculations averaged across the plateau. Measured daily snowmelt is calculated using the initial measurement, of snow height on the ablation string, prior to snowmelt subtracted by the daily measurement. The computed melt rate, used in combination with the areal snow cover depletion from the UAV are used in a non-linear regression to interpolate the loss of snow mass during the days when the site could not be manually measured.

As K↓ is the greatest contributor to Q_m (Haughton, 2018) a comparison of burned to unburned clear-sky conditions was analyzed. The term clear-skies is better defined as 'mostly clear-sky' as data for perfectly clear-skies are rare. Clear-sky conditions we're determined using a micrometeorological tripod within a bog at Scotty Creek which has been running since 2004. It was assumed that during those 13 years there was at least one relatively cloud-free day for each Julian day. These values represent the maximum expected incoming radiation on a cloud free day.

An 80% of the maximum expected incoming radiation was used as a threshold value for clear-sky to increase the dataset as the tripods on the burn and unburned plateau which are within a forest canopy and have the effect of tree shading.

2.4 – RESULTS

2.4.1 – Impacts of Fire on Winter Processes

One year post-fire snowpack distribution and duration

During the 2014-2015 snow year, peak SWE accumulation occurred on 09 April 2015 (Figure 4). There were significant ($p < 0.05$) differences between measured end-of-season (29 March - 03 April) average SWE at the burned and the unburned portions of the peat plateau. Leading to a greater SWE on the burned plateau at the beginning of the snowmelt period (05 May; Figure 4). A 26% increase of SWE at the burned plateau is due to the significant increases of both snow depth (16% increase) and density (8% increase). SWE remained significantly greater on the burned plateau throughout the intermittent melting and snowfall period (05 – 16 April), during this period the snowpack is densifying and sublimating, in other words priming for snowmelt (Figure 4). The continuous snowmelt period began (17 April), when night time air temperatures were no longer cold to sufficiently refreeze the snowpack.

During this period of continuous melting, the burned plateau snowpack SWE remains greater than the unburned plateau until snow free patches begin to present themselves on the landscape. Percent snow covered area (SCA) indicates the first snow-free patches occurred on the unburned portion of the plateau (18 April) as evident by the rapid drop in the SCA prior to the burned side (Figure 5a). The snow-free patches initially form as depressions around the base of

tree trunks, resulting from the emission of longwave radiation (L↑) from the trees, and shallower snowpack due to the efficiency of canopy interception and sublimation.

Although snow-free patches were first to occur in the unburned study plateau, complete snowpack disappearance occurred four days earlier on the burned plateau (Tableau 4). Once snow-free patches began on the burned plateau (20 April) the SWE began to drop significantly faster than the unburned plateau (Figure 5). Final snow-free day on the burned site occurred during the period when the site was inaccessible, for this reason SCA acquired by UAV imagery was used to infer the final snowmelt date.

The first snow-free day observed by SCA and calculated from a regression analysis of measured SWE were the same (Figure 5b), however during the snowmelt period the computed trend did not follow the trend set by the observed data. The relationship between SCA and measured SWE from snow surveys, provides an estimate of the latter value from the former when the site was inaccessible, and was used to infer the SWE and snowmelt rates during the measurement hiatus, as represented by the dashed lines on Figure 4, post 27 April 2015.

SWE during this the second half of the continuous snowmelt (Figure 4) was interpolated from a linear regression (Figure 5b) from days prior to the inaccessible date on days when both snow survey and the UAV were flown. Average SCA depletion rates (10 April to 10 May 2015) were 31.1% greater in the burned forest than the unburned forest, while the maximum measured single day (on 01 May) SCA depletion rate was 24% greater (Figure 5) in the burned forest than in the unburned forest.

Snowmelt energy

Snowmelt rates (M) are greater on the burned plateau (Table 4) due an increase (27.5%) in the energy available to melt the snowpack (Q_m) earlier (20 April) in the continuous snowmelt period (Figure 6). Early Q_m is weighted by the snow-free pixels from the SCA, as snow-free patches grew the percentage of the Q_m over the landscape decreased as energy is transferred to the ground heat flux (Q_g). In the burned forest, daily average Q_m peaked (26 April) five days earlier than in the unburned forest (Figure 6a). Loss of the canopy increases in incoming shortwave energy (K↓) which proportionally increases the energy available for melt. Although the peak of the daily average Q_m was slightly higher in the unburned forest, cumulative Q_m (Figure 6b) in the burned forest was 35.2% greater, allowing the burned forest to become snow-free four days earlier than the unburned forest (Table 4). Average daily M in the burned forest was increased 40% than the unburned forest, which aligns with previous research on snowmelt rates in burned forests (Winkler, 2011; Burles and Boon, 2011).

Of the components of Q_m in Equation (1), the only statistically significant differences ($p < 0.05$) between the burned and unburned forest sites were the mean sensible (Q_h) and latent (Q_e) heat fluxes. The Q_h, is directionally proportional to the K↓, Q_h accounting for 20% to 38% of K↓ (Chambers and Chapin, 1999; Yoshikawa *et al.*, 2002). K↓ has been shown to be the greatest component contributing to snowmelt in subarctic boreal forests (Haughton, 2018). Cloud-free (80^{th} percentile) cumulative K↓ during the snowmelt season (April 2015) was significantly lower (89.23 MJ m^{-2}) in the unburned forest than the burned forest (257.26 MJ m^{-2}) due to higher amounts of radiative filtering provided by the unburned black spruce canopy. Snow albedo is significantly greater at the burned forest than the unburned forest (Figure 7), reducing the amount of shortwave

radiative input to the snowmelt energy balance. However is offset by an increase in emitted longwave radiation from the dead charred tree trunks.

Albedo

The burned and unburned forests exhibited significant differences in albedo during the snowmelt (Figure 7) and summer periods (Figure 8). During snowmelt (02 April to 30 April), the average albedo in the unburned forest (0.32) was lesser than the burned forest (0.42) due to litterfall from the living canopy (Figure 7). After snowpack disappearance (05 May), the blackened surface of the charred trees increased the absorption of solar radiation and resulted in the burned forest (0.01) having a lower average monthly albedo than the unburned forest (0.11). There is a dampening of the albedo difference between the two sites in the summer of subsequent years after the burn, as the understory begins to re-establish. Leading to less variation in daily maximum albedo on the burned site.

2.4.2 – Impacts of Fire on Summer Processes

Ground thaw and frost table development

In 2015, early spring (10 May) average FT depths in the burned forest were 25 cm (± 9.4 cm) and were not significantly different than the unburned (20 ± 10.3 cm) forest (Figure 9a). There was, however, significant intra-site FT depth variability within each characteristic land cover feature owing to differences in microtopography, moisture content and vegetation structure (Figure 10). The relative frequency of FT depth is log-normally distributed (Figure 10a) on both the burned and unburned portions of the study plateau. In late spring (03 June), FT depths on the unburned

plateau ranged from 20 to 80 cm, with the majority (89%) occurring between 20 cm and 40 cm (Figure 10b). The majority of FT depths in the burned forest (96%) in late spring were distributed between 40 cm and 80 cm, but the distribution was skewed to include some thaw depths of up to 140 cm. In early summer (26 June), FT depths in both the unburned and burned forests were normally distributed from 20 to 140 cm, and 40 to > 200 cm, respectively (Figure 10c).

There was no significant difference between the shallowest FT depths in the burned and unburned forests throughout the thawing season (Figure 9a). The deepest FT depth in the unburned forest never exceed 150 cm throughout the thawing period, however maximum FT depth in the burned forest exceeded 150 cm continuously after 20 June (Figure 9a), and exceeded 200 cm when final FT measurements were taken at the end of August 2015.

Ground cover effect on thaw

FT depths varied over time and space on both the burned and unburned portions of the peat plateau (Figure 9a). Spatial variations of thaw depths within a forest canopy are due to changes in micro-topography and vegetation cover (Figure 11). On the unburned plateau, average suprapermafrost layer thickness (SLT) under different vegetation covers are not significantly different (Figure 11). However, the SLT in open, charred peat on the burned plateau was much more variable and was significantly different than the two other classes (Figure 11).

Soil temperature

Average unburned soil temperatures (T_{soil}) were significantly warmer than burned T_{soil} throughout the soil profile (0, 8, 16, 32 and 64 cm) in the winter of 2015-16 (Table 5) despite the

increase in snowpack depth on the burned plateau. Warmer T_{soil} overwinter on the unburned plateau are attributed to the radiative heat transfer from the living roots of the black spruce on the unburned plateau. At depths of 64 cm the burned site in winter 2015 is warmer (Table 4), due to the heat released from storage lower in the profile.

At the ground surface (0 cm), T_{soil} were significantly higher at the burned site than the unburned site during the 2015 and 2016 summers (Figure 12, Table 5), likely due to the blackening of the surface and decreased albedo (Figure 8). During the summer of 2015 and 2016 at depth of 64 cm maximum T_{soil} we're significantly warmer on the burned portion than the unburned portion of the peat plateau (Figure 12).

Significantly warmer temperatures at greater depth on the burned plateau are indicative of greater potential thaw depths as T_{soil} provide an indication of the physical state of pore water within the soil. At Scotty Creek, the freezing point depression is about -0.3°C (Quinton and Baltzer, 2013), and depending on moisture content and depth, soil may remain in the zero-curtain between two weeks and the entire winter (Connon *et al*., 2018). Spring T_{soil} in the burned forest breakout of the zero-curtain period on average three days later than the unburned forest (Table 6). In the burned forest, T_{soil} at 16 cm depth froze five days earlier than the unburned forest (Table 6), thereby fundamentally changing the subsurface hydrologic and thermal regimes.

2.4.3 – Impacts of Fire on Talik Development

Multi-year end-of-winter snowpack distribution

One year post-fire (2015) was an above average snow year (167 mm), relative to 30 year climate normals (143 mm) at the Fort Simpson A station (ECCC, 2017). Two years post-fire (2016)

was an average snow year (150 mm), receiving 105% of normal conditions. While three years post-fire (2017) was below average (109 mm), receiving 76% of normal conditions. In the 2014-2015 snow year, there were two relatively large snowfall events (> 15 mm) in mid-October (2014) that insulated the ground from cold winter temperatures. By the end of November 2014, 61 mm of SWE had accumulated on the ground surface. By contrast, the 2016-2017 snow season did not receive that amount of SWE until mid-February. Early season snow accumulation patterns were similar between the 2014-2015 and 2015-2016 snow years.

Suprapermafrost layer taliks

Soil temperatures at 64 cm depth in the burned forest were significantly warmer than the unburned forest during the 2015 and 2016 summers (Table 5). While overwinter T_{soil} at 64 cm in the burned site did not breakout of the zero-curtain period, implying that a perennially unfrozen talik is present at this depth. A study by Connon *et al*. (2018) at Scotty Creek, who found typical refreeze depths in the winter of 2015 to be between 0.5 and 0.7 m. These authors also found that refreeze depth never exceeded 0.8 m, suggesting that summer thaw depths exceeding this critical threshold would not completely refreeze. Given this information, it is therefore inferred that thaw depths of > 0.8 m are indicative of the presence of a suprapermafrost talik. Connon *et al*. (2018) also found that, once established, areas with a suprapermafrost talik experience thaw rates nearly five times greater than those without taliks. By the end of summer of 2015 (26 August), many FT depths on the burned (44%) and unburned (40%) peat plateau were between 0.6 and 0.8 m (Figure 10d). On the burned plateau, 41% of the FT depths were deeper than 0.8 m, while only 20% were deeper than 0.8 m on the unburned plateau.

Three year post-fire comparison

At the grid sites, average SLT in the burned forest has increased progressively each year since the 2014 fire; whereas average SLT in the unburned forest has remained relatively stable (Figure 13a). Furthermore, the number of points in the grid on the burn with an SLT exceeding 0.8 m has increased from 24% to 57% over the three years. The number of points on the unburned plateau with an SLT exceeding 0.8 m has remained constant at 41%.

Average SLT on the burned plateau 3 years post-fire is 20.8% (15 cm) greater than 1 year post-fire while the unburned plateau SLT is only 16.2% (11 cm) thicker. One-year post-fire (2015) average SLT on the burned plateau increased 5.9% compared to the unburned plateau the same year, while three-years post-fire the plateau difference has almost doubled and the burned plateau SLT is 10.1% deeper than the unburned plateau.

Average soil moisture within the top 20 cm of the soil profile (Figure 13b) in 2016 is significantly lower than 2017 on both the burned (37.5% difference) and unburned (48.65% difference) portions of the peat plateau. In both two- and three years' post-fire, the burned plateau is significantly drier than the unburned plateau.

2.5 – DISCUSSION

By changing the physical properties of the ground surface, fires can have a significant impact on energy cycling in the suprapermafrost layer and the permafrost body (Kasischke *et al.*, 2012; Walvoord and Kurylyk, 2016; Yoshikawa *et al.*, 2002). In areas underlain by extensive discontinuous or continuous permafrost, where permafrost temperatures decrease considerably lower than the freezing point depression, the zone between the base of the suprapermafrost layer and the depth of zero annual amplitude undergoes temperature change on an annual basis (Muller, 1947). In conditions where permafrost is stable, energy that is conducted to the permafrost body in the summer is lost during the winter and this energy exchange is evident by changes in temperature. However, at the Scotty Creek study site and other areas of sporadic discontinuous or isolated permafrost, the temperature of the entire permafrost body is commonly at, or very close to, the freezing point depression (see Table 1). Here, energy conducted into and out of the permafrost body is used as latent heat and is not detected as a change in temperature. Winter and summer time permafrost energetic work in combination to increase the suprapermafrost layer thickness leading to greater permafrost thaw as broken down in a conceptual model (Figure 14) representing the results of this study and further discussed below.

2.5.1 – Winter Permafrost Energetics

In this study of a low-severity burn, snow cover water equivalent at the burn site was 26% higher than the unburned site (Table 3). As shown in other studies these differences become greater as the severity of the fire increases (see Table 2). The increased snow cover provides thermal insulation to the underlying permafrost body and restricts overwinter energy loss (Figure 14). However, the burned canopy and loss of foliage allows for enhanced ventilation and increases the

transfer of turbulent fluxes over the snowpack. Enhanced ventilation allows for cooler air temperatures and increases the thermal gradient between the ground surface and the snowpack. Colder overwinter ground temperatures were observed on the burn site down to 64 cm (Table 5), suggesting that enhanced ventilation has a stronger impact than increased snow depth on the overwinter ground heat flux.

The burned forest also allows for increased transmissivity which provides energy for more rapid snowmelt increasing the duration of a positive heat flux into the subsurface (Table 6). Significant increases in the incoming shortwave energy proportionally increased the energy for melt, therefore leading to greater average snowmelt rates on the burned plateau. Despite the low-severity of the burn in this study, there was a significant difference in snowmelt rates between the burn and unburned portions of the peat plateau. Previous studies with comparable snowmelt rates on the control have shown further increase of snowmelt rates with increasing fire severity (Burles and Boon, 2011).

Overwinter ground surface temperatures in the burned forest were consistently colder than those in the unburned forest. When soil temperatures drop below the freezing point depression (-0.3°C) they enter the zero-curtain phase, the latent heat release required to freeze the soil has been exhausted and the soil can be presumed frozen. Soil freezing greatly reduces the hydraulic conductivity of soil (Woo, 2012) and increases the thermal conductivity (Farouki, 1981), allowing for more rapid energy loss from the ground, as indicated by the increase in negative ground heat fluxes overwinter (Figure 14). Ground temperatures at 32 cm did not break out of the zero-curtain phase on the unburned plateau however they did on the burned plateau, indicating that there was incomplete freezing at this depth and suggests talik development.

The development of a talik between the active layer and permafrost body decouples the permafrost from the snowpack and atmosphere, as there is a continuous (although small) downward thermal gradient throughout the winter (Figure 14). Increasing number of taliks in the burned forest (Figure 13a) indicate the changes to the ground thermal regime, initiated by fire are perpetuated in subsequent years after the disturbance. It is hypothesized that as talik networks grow and coalesce, the subsurface movement of water and associated advective transport of energy will facilitate more rapid thaw of the underlying permafrost. The growth of the taliks, increases the distance between the active layer and permafrost table further attenuating the effects of the downward thermal gradient in winter.

In summary, although energy loss from the ground surface appears to be greater in the burned forest, this effect does not propagate to the permafrost table, which is thermally buffered by a talik. In colder climates where the permafrost table is closer to the ground surface, forest fires may result in enhanced energy loss from the permafrost body in the winter, but this effect may also be mitigated by a thinner tree canopy.

2.5.2 – Summer Permafrost Energetics

Changes to the physical properties of the forest canopy and ground surface alter how much energy is available for ground thaw, and how that energy is conducted through the subsurface. Thinning of the tree canopy increases transmissivity of shortwave radiation and a decrease in albedo caused by the charred trees increases emitted longwave radiation; both increase the net radiation flux at the ground surface (Figure 14).

As soil moisture is a key variable in determining thaw depth in peatland terrains (Williams and Quinton, 2013), it is necessary to understand how soil moisture changes in response to forest fires, and then to evaluate the relative consequences of increased transmissivity against changes to soil moisture. Transpiration in the burned forest is reduced because of non-living trees, however sap-flow rates in black spruce (*Picea mariana*) are low enough to not significantly reduce soil moisture in the burned forest. Conversely, the increase in available energy at the ground surface enhances evaporation from capillary-held water within the soil. The increase in evaporation appears to outweigh the decrease in transpiration, as soils in the burned forest are generally drier than soils in the unburned forest (Figure 13b). As a result, the bulk thermal conductivity in the burned forest soil is lower than the unburned forest, potentially limiting thaw depth, which are strongly correlated to soil moisture (Wright *et al.*, 2009).

However, thaw depths in the burned forest are significantly greater than thaw depths in the unburned forest (Figure 13a), suggesting that the increased energy availability outweighs the impacts of a drier soil. Our data shows that the increased ground heat flux in a burned forest in the summer is more substantive than the small increase in energy conducted out of the ground over winter (Figure 14). The increases in the ground heat flux in summer are attributable to greater inputs of solar radiation and decreased albedo, hence forth increasing summer soil temperatures, at the surface and in depth (Figure 12), leading to greater thaw depths below charred vegetation cover (Figure 11). The aforementioned processes in association with an increased snowmelt rate and earlier onset of the thawing season (Figure 4) due to greater energy available for snowmelt (Figure 6), substantially increase the energy available to melt the soil ice content (Figure 9), further deepening the suprapermafrost layer annually (Figure 13a). Therefore, the perturbation caused by a low-severity fire appears to be strong enough to induce talik development in a peatland terrain

underlain by discontinuous permafrost, despite the increased depth of the snowpack and potentially greater insulation as well as reduce thermal conductivity from drier soils on burned peat plateaus.

2.5.3 –Talik Development

It has been well documented that the net effect of a severe forest fire leads to an increase in thaw depth resulting in talik formation (Brown *et al*., 2015). However, it has also been shown that these features are transient over time, and that over a period of 30 to 40 years, the permafrost returns to a stable state (Smith *et al*., 2015). However, in the study areas and other regions of discontinuous and sporadic permafrost climatic warming, being greatest in Northwestern Canada, increases in air and soil temperatures leading to greater annual thaw depths and permafrost degradation (Figure 15).

As thaw depths increase yearly and the active layer deepens past the overwinter refreeze depth, taliks begin to form. In a study of talik development on natural (i.e. unburned) peat plateaus at the Scotty Creek study site, Connon *et al*. (2018) found that once taliks are initiated, complete degradation of the underlying permafrost is very likely (Figure 15a). Once a talik has been established the active layer decreases due to the thermal conduction of these perennially unfrozen and saturated taliks below the active layer and above the permafrost table. The overwinter presence of the taliks within the suprapermafrost layer indicates a continuous degradation and warming of the permafrost table. As forest fires effects on above and below ground energetics accentuate thaw depths, taliks are formed sooner and in larger proportions than would be expected in a climatic warming scenario.

Permafrost degradation in areas with taliks are approximately five times faster than areas without taliks (Connon *et al.*, 2018). Our data show similar trends, as thaw depths in the burned forest have increased each of the three years since the fire (Figure 13a). We propose that given the current warming trend, and that permafrost in this region is thin (< 10 m) and relatively warm (> -1°C), that low-severity fires can sufficiently alter the thermal regime enough to trigger complete permafrost thaw (Figure 15b).

2.6 – CONCLUSIONS

This study examined the effects of a mild fire on a peat plateau in a discontinuous permafrost wetland of the southern Northwest Territories three years post-fire. Changes in forest structure resulted in a deeper snowpack, greater SWE, and more energy available for snowmelt in the burned forest compared to the unburned forest. The greater availability of energy for snowmelt in the burned forest is driven by a combination of factors, such as the latent and sensible heat fluxes, incoming and emitted short- and longwave energy. Snow albedo may be mitigating the snowmelt rates on the burned forest. Despite the higher albedo, the snow surface temperatures were warmer on the burned forest snowpack rather than the unburned forest, because of a greater transfer of heat from the surrounding trees and heat advection from open patches, further increasing the melt rate.

Despite the greater snowpack depth on the burned site, as well as the greater suprapermafrost layer thickness, no significant correlation was found to indicate that an increase in snow depth overwinter has a significant and direct impact on the rate and depth of thaw. Increased rates and depths of thaw are likely due to a combination of factors: (i) a longer thawing

period due to the snowpack disappearance earlier on the burned portion; (ii) an increase in energy available for thaw caused by the greater input of incoming shortwave energy from the lack of canopy and emission of longwave energy from the charred trunks, and (iii) decreased albedo, contributing to the warmer soil temperatures at greater depth on the burned portion than the unburned. The combination of the aforementioned factors leads to the creation of taliks, which increases depth of thaw the following years post-fire.

Few studies have previously shown the effects of fires on snow accumulation and snowmelt, and their effects on seasonal ground thaw is rarely referred to (Table 1). Understanding snowmelt and ground thaw in remote northern areas is important as the landscape is modified with future climatic changes. The importance of taking burned areas into account when modeling for snowmelt and ground freeze/thaw cannot be ignored as this study has shown a minor fire can create minimal changes to the energy balance, which will significantly increase snowmelt and ground thaw rates. Further studies on the effects of a more severe burn, or a period greater than two years, could provides different results in the discontinuous wetland. Additional studies could improve large-scale runoff models for burned peat plateaus, within the wetland environment.

Table 1. Summary table of ground thaw studies in various forest types with discontinuous permafrost (PF) coverage under a range (Low, Moderate and High) of fire severity. Looking at pre- and post-fire organic layer thickness (OLT), FT and PF depths and soil temperatures (T_{soil}). Variables are represented as either a range (MIN to MAX) and/or as an average with or without standard deviations ([average ± StDev]).

	Mathieu *et al*., 2018	Smith *et al*., 2015	Brown *et al*., 2015	Kopp *et al*., 2014	Jorgenson *et al*., 2010	Yoshikawa *et al*., 2002
Burn Year	2014	1994	1930 - 2010	---	---	1924 - 1999
Study Year(s)	2015 - 2017	1995 - 2012	2011 - 2014	2011 - 2012	1998 - 2001	1996 - 2000
Location	Southwestern NWT	Central Mackenzie Valley NWT	Interior Alaska	Sugnugur basin, Mongolia	Central Alaska	Interior Alaska
Mean Annual Air Temperature	-2.8℃ (1981 - 2010)	-5.1℃ (1981 - 2010)	-3.7℃ (1971 - 2000)	-2.4 (2011 - 2012)	-2.2℃ (1997 - 2007)	-2.2
Total Annual Precipitation	388 mm	294 mm	323 mm	354 mm	---	222 mm
Δ Snow Depth (% increase)	16%	17 - 21%	---	---	25%	Not significant
PF Coverage	Discontinuous	Discontinuous	Discontinuous	Discontinuous	Discontinous	Discontinous
Dominant Tree Species	Open Black Spruce	White Spruce and Birch	Closed Black Spruce	Siberian Pine and Larch	Black Spruce	Black Spruce and Birch
Fire Severity[1]	Low	Low to Moderate	Moderate to High	Low to High	Moderate	Low to High
OLT (cm)						
Control	> 30	58	89 to 176	---	30	15 to 25
Burned	---	Low 50 Moderate 25	Moderate 7 to 14 High 2	4 to 8	14	Low 15 Moderate 13 High 3
Soil moisture (% vol)[2] at depths	20 cm	60 cm		20 cm	15 cm	
Control	18.8 ± 6.5	32.7	37 to 43	12.6 ± 0.0027	19 to 72 [51]	23.6 ± 7.08
Burned	13.2 ± 6.3	Low 42.0 Moderate 61.2	Moderate 13 to 56 High 65	8.43 ± 0.0034	20 to 69 [48.3]	Low 35.7 ± 13.0 High 31.8 ± 6.1
Δ thaw depth (cm)	10	12	---	14	42	12.6
PF table depth (m)[3]						
Control	1.4		3	1.2 to 1.5	0.68	0.6 to 0.7
Burn	> 2.0	Low 1.10 Moderate 1.25	Moderate 7.6 High >10	3	1.10	Low 0.98 High 3.4 to 4.15
Δ AVG surface Tsoil (℃)	1.5 to 2.0	1.96 to 3.54	2.0 to 3.0	4.3	2.0	2.0 – 3.0
AVG Tsoil (℃) at depth	64 cm	1 m		30 cm	2 m	1 m
Control	1.8 to 2.0	0.7	---	2.7	-1.2℃	3.0 to 3.5
Burn	3.5 to 3.6	1.4 to 1.7	---	4.5 to 7.2	-0.1℃	1.5 to 2.0

[1] Fire severity when not indicated in the study is determined based on OLT defined by Brown *et al*. (2015); unburned (30 cm) low severity (15 cm), moderate severity (7 cm), high severity (≤ 2 cm)
[2] Soil moisture was measured various ways in different studies: Mathieu *et al.* (2018), measured integrated 20 cm GWC. While other studies measured at specific depths. Brown *et al.* (2015) measured GWV integrated throughout the AL, depth varied depending on burn severity. *NOTE* Kopp *et al.* (2014) measured VWC which was converted in this study for comparison purposes using bulk densities (BD) from Benscoter *et al*. (2011); BD @ 10 cm UB 22 and B 37. Volumetric water content (VMC; m3 m-3) x bulk density = % moisture by volume
[3] PF table depth was not measured in Kopp *et al*. (2014) on the burned site, maximum VWC was used as a proxy to PF table depth.

Table 2. Summary table comparing this study and others in various forest types, and different fire severity across western North America. Studies, similar to this one measured forest characteristics, snowmelt rate and timing.

	Burles and Boon (2011)	Winkler (2011)	Skidmore *et al.* (1994)	Spittlehouse (2008)	Mathieu *et al.* (2018)
Burn Year	2003	2003	1988	Simulation	2014
Study Year(s)	2009 - 2010	2004 - 2008	1993	2002 - 2007	2015
Location	Southern AB	South-central BC	Montana, USA	South-central BC	Southwestern NWT
Permafrost Coverage	None	None	None	None	Discontinuous
Fire Severity	High	---	---	Low-High	Low
Dominant Tree Species	Subalpine Fir	Mature Lodgepole Pine	Mature Lodgepole Pine	Mixed Mature Pine and Spruce	Black Spruce
Average Tree Height (m)					
Burn	8.6	23	10.6	23	2.2
Control	9.9	23	11.3	23	2.2
Transmissivity[1] (%)					
Burn	82	77 to 83	---	35 to 80	80
Control	9	16	---	15	50 to 60
Average SWE (mm)[2]	173.1	295.0	---	240 to 350	186.24
Δ Snow Cover (%)[3]	50 to 58 [54][4]	-23 to 77 [25]	7	---	24
Snowpack Disappearance (days)[3]	8 to 14	4 to 15* [11]	6	7 to 16	4
Snowmelt Rate (cm/day) - Range [average]					
Burn	1.28 to 1.54 [1.28]	1.15 to 1.87 [1.46]	---	---	0.60 to 0.80 [0.73]
Control	0.50 to 0.70 [0.56]	0.71 to 1.02 [0.91]	---	---	0.10 to 0.69 [0.52]
Δ snowmelt rate (%)[3]	44 to 46	60**	57	10 to 35	40

[1] Burned transmissivity not measured in Mathieu *et al.* (2018); instead measurement indicates sparse spruce stands while control transmissivity is a dense black spruce canopy.
[2] Average SWE was not listed in Skidmore *et al.* (1994), but 25 year average snow depths are 117 cm. Spittlehouse (2008), 240 and 350 mm, are yearly maximum and minimum measured over a five year period.
[3] Expressed as increases over the control (*i.e.* unburned) conditions.
[4] Indicates the "Range [Average]".
* Decreases steadily post-fire. 15 days was the difference in the first year post-fire.
** Calculated from the Δ snowmelt rate measured by Winkler (2011) where it is 38% lower on the control.

Table 3. March to August monthly average temperatures and precipitation for 2015 compared to the 30 year (1981-2010) climate monthly normals from Environment Canada's station Fort Simpson A (MSC, 2016).

	Temperature (°C)		Precipitation (mm)	
	2015	1981-2010	2015	1981-2010
March	-10.7	-13.0	13.2	15.4
April	1.0	-0.4	27.4	17.0
May	12.4	8.7	9.0	29.4
June	16.0	15.3	11.7	51.3
July	16.9	17.4	73.3	61.1
August	14.8	14.7	53.4	61.4

Table 4. Snowmelt period characteristics including the end date of snowmelt represented by the snow-free (SF) day, energy for available for melt of the snowpack (Q_m), the melt rate over the snowmelt period, as well as total loss of snow water equivalent (SWE).

Snowmelt characteristics	Burned	Unburned
Snow Free Day	05 May	09 May
Cumulative Q_m on SF day (MJ m^{-2})	196.2	144.8
Melt rate (cm day^{-1})*	0.7	0.5
Total loss of SWE (mm)	202	172

*Calculated from 05 April 2015 to the respective snow-free days for each site.

Table 5. Average seasonal air and soil temperatures on the burned and unburned peat plateau for different seasons from 2015 to 2016. Summer is defined as 01 April to 31 October, while winter is 01 November to 31 March. Bold numbers indicate statiscially significant differences between the burned and unburned seasonal average soil temperatures at the indicated depth.

Depth (cm)	Summer 2015		Winter 2015		Summer 2016	
	B	UB	B	UB	B	UB
Air	12.3	12.1	-14.8	-14.9	15.8	15.8
0	**12.3**	**10.8**	**-2.5**	**-1.7**	**16.9**	**14.9**
8	10.9	11.8	**-1.5**	**-1.0**	**16.7**	**15.4**
16	8.6	9.5	**-0.9**	**-0.5**	**12.5**	**13.7**
32	5.7	6.1	**-0.2**	**-0.1**	**7.0**	**8.7**
64	**3.5**	**1.8**	**0.0**	**0.0**	**3.6**	**2.0**

Note: Winter 2015 soil temperatures at 64 cm were significantly different as the values were -0.002 ± 0.025 ℃ and 0.034 ± 0.007 ℃, respectively for the burned and unburned plateaus.

Table 6. Zero-curtain period as expressed by the start and end dates as well as the duration (days) for spring 2015 and 2016, and fall 2015 on the burned and unburned portion of the burned plateau at 0, 8, 16, 32, and 64 cm.

Depth (cm)		Spring[1] 2015		Fall[2] 2015		Spring 2016	
		Date[3]	Duration	Date	Duration	Date	Duration
0	B	--- **06 APR**	---	08 OCT 09 OCT	1	14 APR **17 APR**	3
	UB	24 MAR **04 APR**	10	07 OCT 24 OCT	17	25 MAR **14 APR**	20
8	B	--- 05 APR	---	09 OCT 26 OCT	17	13 APR **17 APR**	4
	UB	14 MAR **05 APR**	22	24 OCT 29 OCT	5	25 MAR **13 APR**	19
16	B	--- 05APR	---	25 OCT 09 NOV	15	23 MAR **16 APR**	24*
	UB	24 FEB **29 MAR**	33	27 OCT 16 NOV	20	23 MAR **13 APR**	21
32	B	N/A[4]		01 NOV 05 JAN	65	15 MAR **14 APR**	30*
	UB	N/A		N/A		N/A	
64	B & UB	N/A		N/A		N/A	

[1] The zero-curtain period in spring is from the first day warmer than 0.3℃ and to the first day warmer than 0.1℃;
[2] The zero-curtain period in fall is from the first day above 0℃ to the first day below -0.3℃;
[3] Bold dates are the first days the soil is thawed at the indicated depth;
[4] N/A indicates the soil hozion never entered a period within the zero-curtain, hence the soil horixon remains unfrozen;
* Longest zero-curtain period given there was a short duration of warming followed by a refreeze before finally thawing. Shorter zero-curtain periods (after the refreezing period) are 13 and 20 days, respectively at 16 and 32 cm.

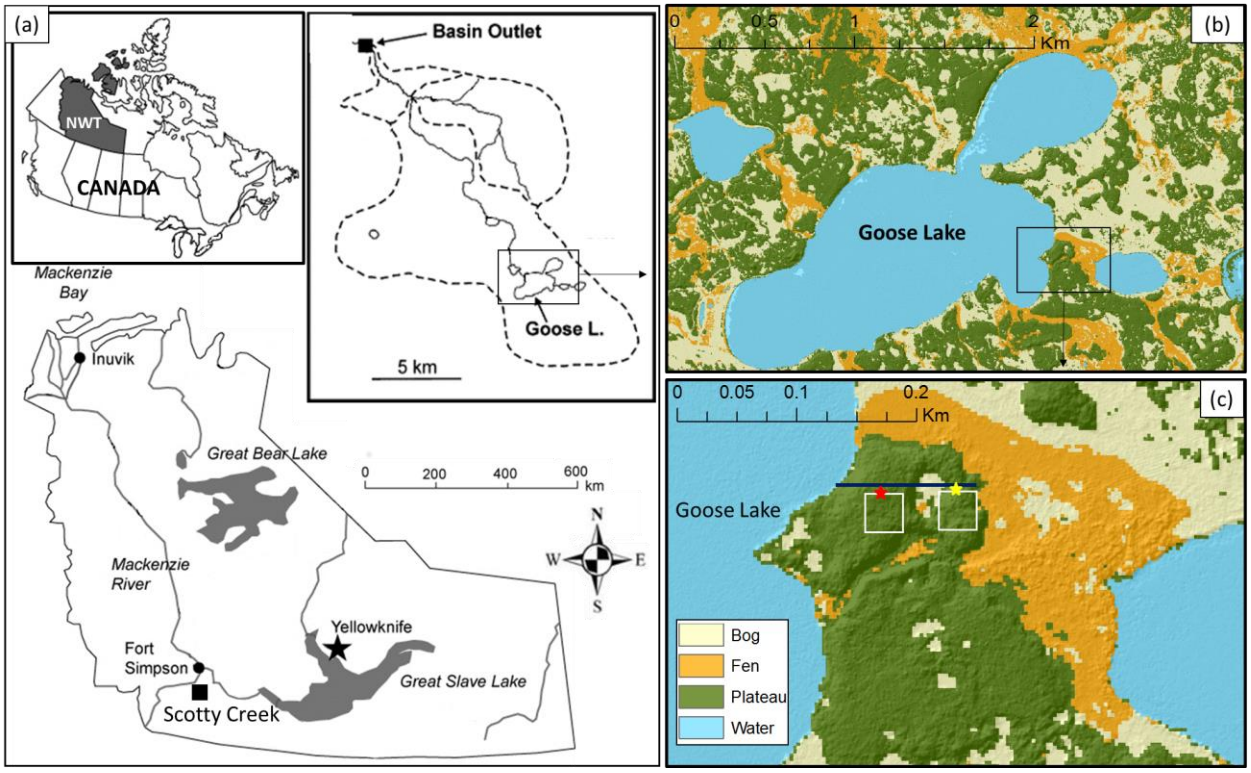

Figure 1. (a) Location of Scotty Creek basin within the Northwest Territories, Canada. Panchromatic WorldView-2 imagery classified by major land cover types representing (b) Scotty Creek fire study site located east of Goose Lake illustrating differences between thermokarst bogs, channel fens and permafrost peat plateaus. (c) The study peat plateau indicating the location of the winter snow survey and summer frost table depth transect (navy line), and the summer frost table depth and soil moisture measurements taken within the grid (white square). Meteorological tripods (star) are located on the north end of the burned (red) and unburned (yellow) grids.

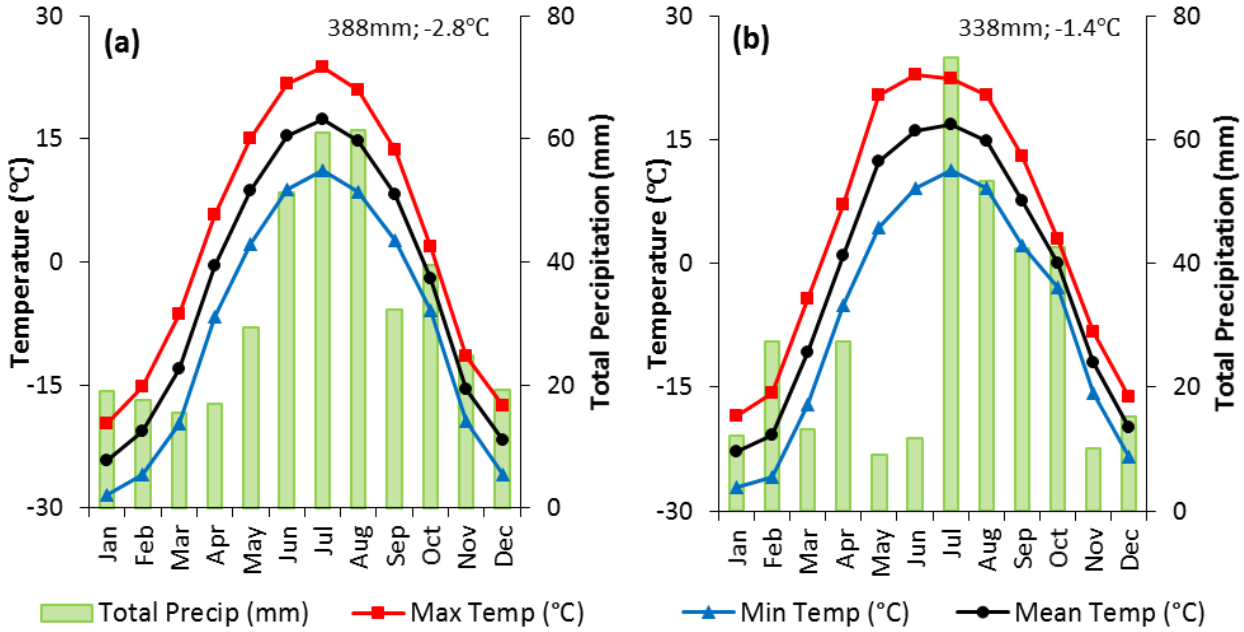

Figure 2. Climate data from Environment Canada station Fort Simpson A (2202101), Fort Simpson, NWT. Monthly minimum, maximum and averaged air temperatures and monthly total precipitation for (a) 1981-2010, 30 year monthly normals, and (b) 2015 (MSC, 2016). The yearly average air temperature in 2015 is warmer than the previous 30 year average; yearly total precipitation in 2015 is less than the average 30 year normals as well.

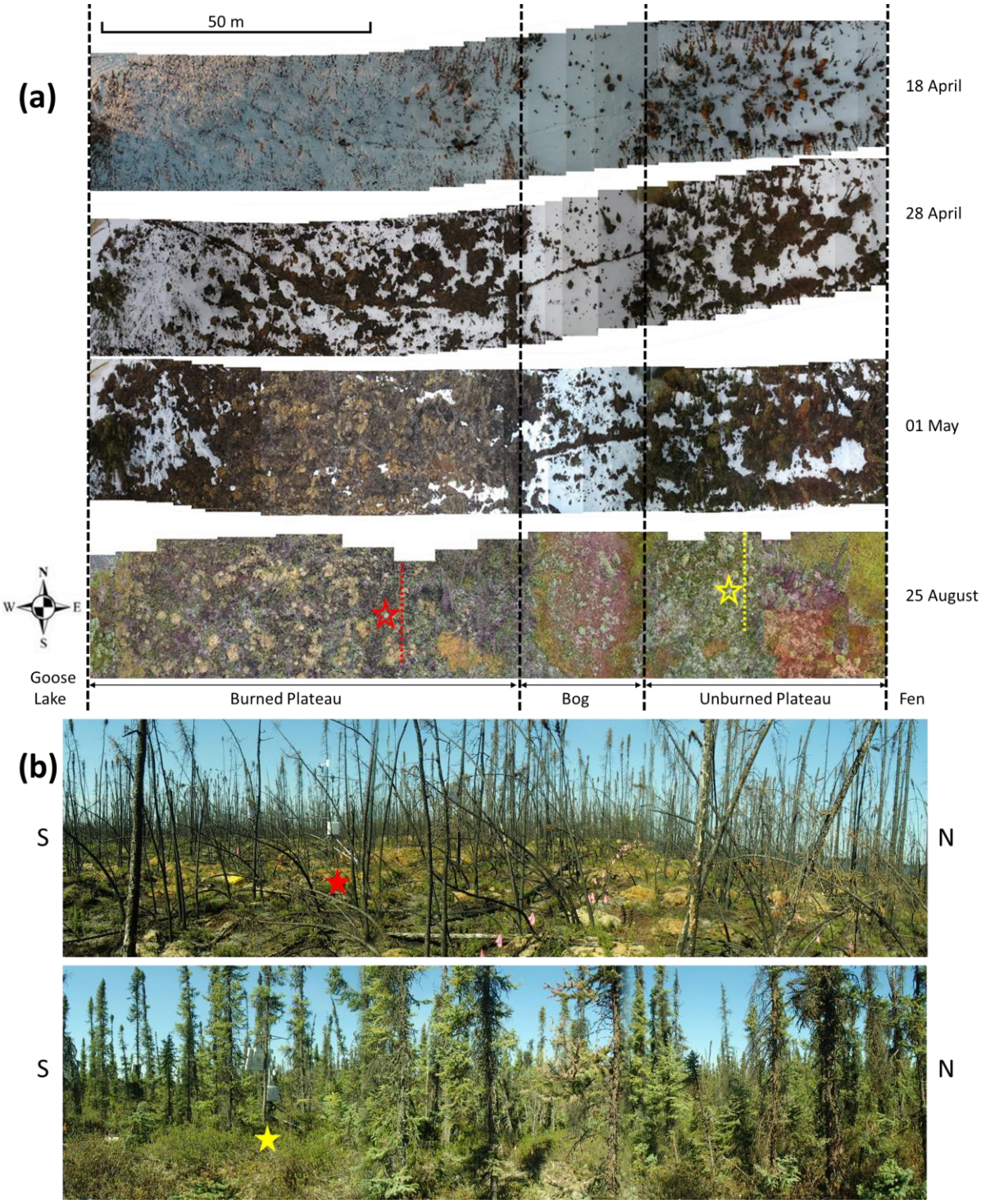

Figure 3. (a) Composite of images from the Phantom Vision 2+ UAV throughout snowmelt on 18, 28 April, 01 May and 25 August 2015, beginning on the left at the edge of Goose Lake on the burned portion of the plateau, crossing over the bog and ending on the right at the fen adjoining the unburned portion of the plateau. (b) Images of the burned plateau (top, red) and the unburned plateau (bottom, yellow) in June 2015, indicating the location of the meteorological tripods (stars) as well as the location of the images (dotted) on the composite images in (a).

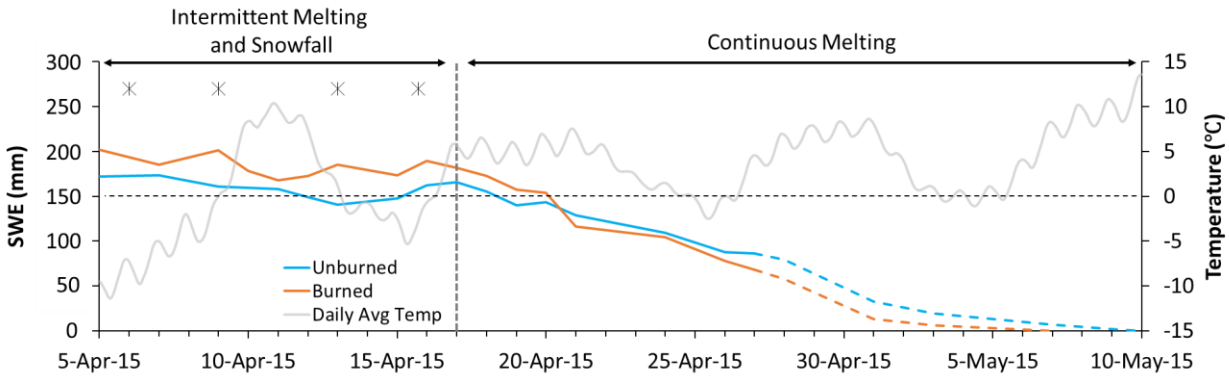

Figure 4. Comparison of the average snow water equivalent (SWE; mm) in burned (orange) and unburned (blue) forest, from 05 April to 10 May 2015. SWE values were measured by snow survey (solid) with SWE extrapolated (dashed) from a non-linear regression of computed snowmelt and areal snow covered area (See Figure 5b). Included are daily averaged temperature (grey) and significant snowfall events (asterisk). The vertical dashed line is the demarcation date (16 April) that separates the "intermittent melting and snowfall" period from the "continuous melting" period, chosen for three conditions; i) after the last significant snowfall event, ii) daily average temperatures remained above the freezing zero point depression, and iii) no overnight refreezing of the snowpack.

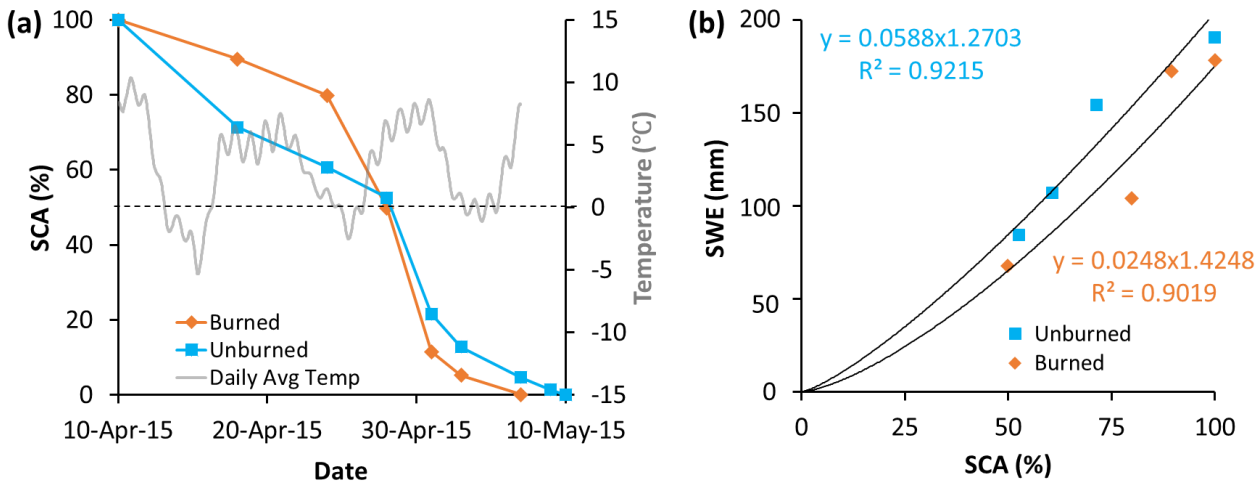

Figure 5. (a) Snow cover area (SCA) depletion curve of a burned (orange) and unburned (blue) peat plateau. (b) Regression equations to extrapolate SWE from SCA. SCA was calculated as percent snow-covered vs percent snow-free pixels from binary UAV imagery acquired bi-daily from 10 April to 10 May 2015.

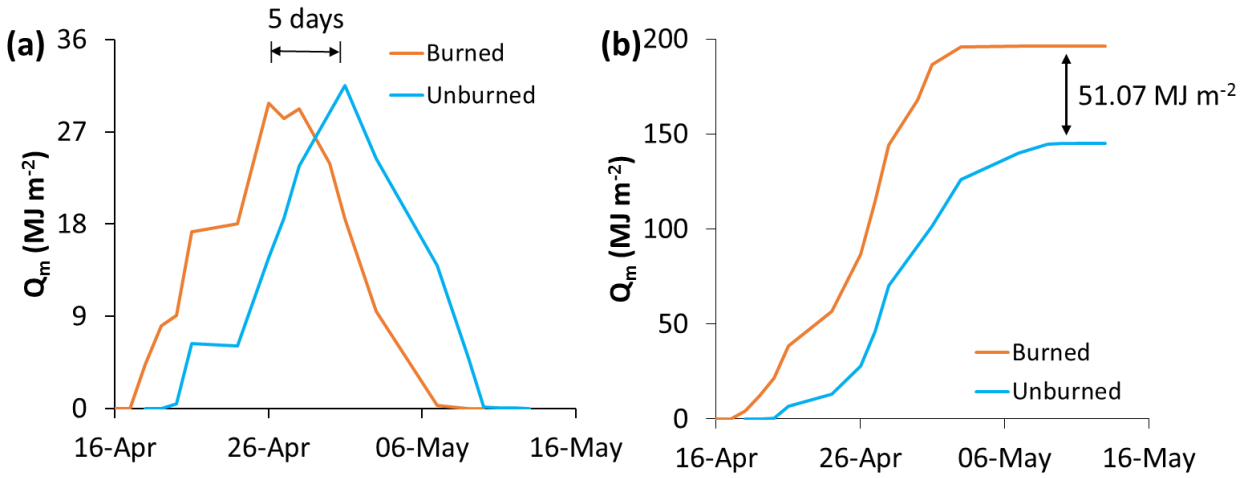

Figure 6. (a) Daily and (b) cumulative energy available for melt (Q_m) computed from an energy-balance model comparing a burned (orange) and unburned (blue) peat plateau during the continuous snowmelt period (16 April to 10 May 2015) as defined in Figure 4.

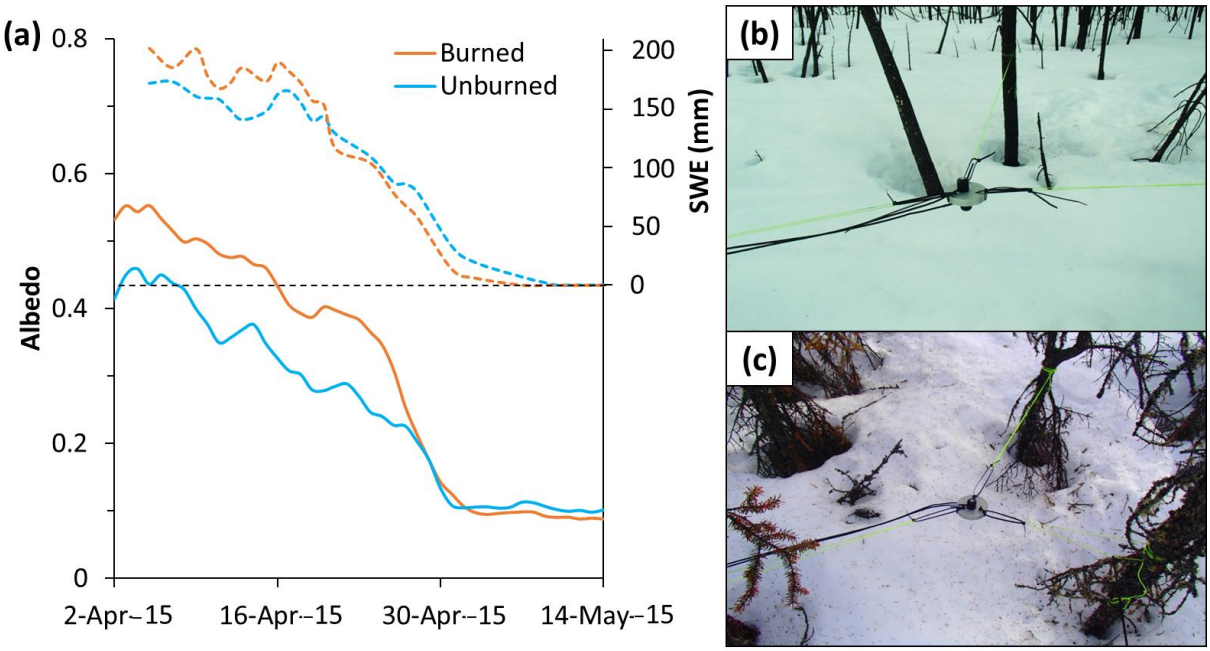

Figure 7. (a) Daily snowmelt snow surface albedo (solid) on a burned (orange) and unburned (blue) plateau beginning 02 April 2015. Snow water equivalent (dashed), through the snowmelt period and into the snow-free period. Spikes in albedo are due to fresh snowfall. Images of the (b) burned and (c) unburned plateau demonstrating visual differences in the albedo due to the cover of debris on the snow surface. Snow surface albedo in 2015 is greater on the burned plateau than the unburned plateau due to the lack of canopy which contributed a greater surface area than the charred debris on the burned plateau.

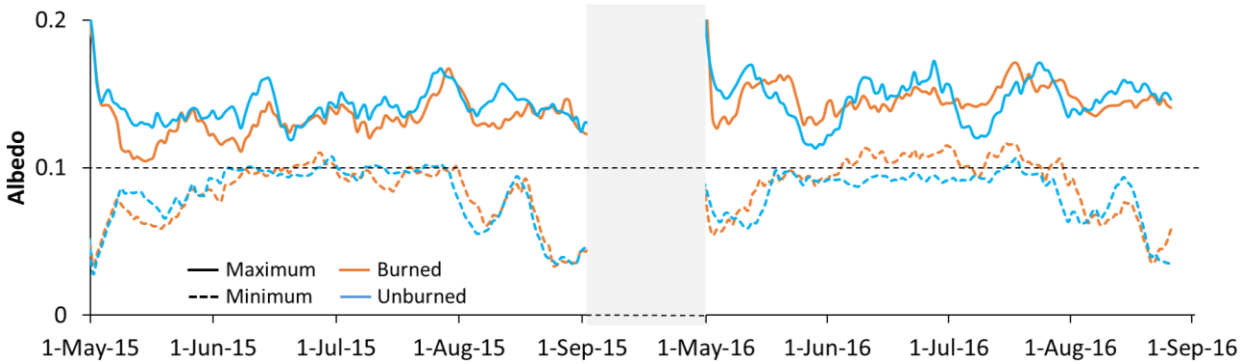

Figure 8. Daily summer (May – September) ground surface maximum (solid) and minimum (dashed) albedo measurements on the burned (orange) and unburned (blue) peat plateau. The grey section between summer 2015 and 2016 is omitted as instrumentation was unsupervised and as such accurate measurements are not certain. No significant differences were found between the burned and unburned plateau.

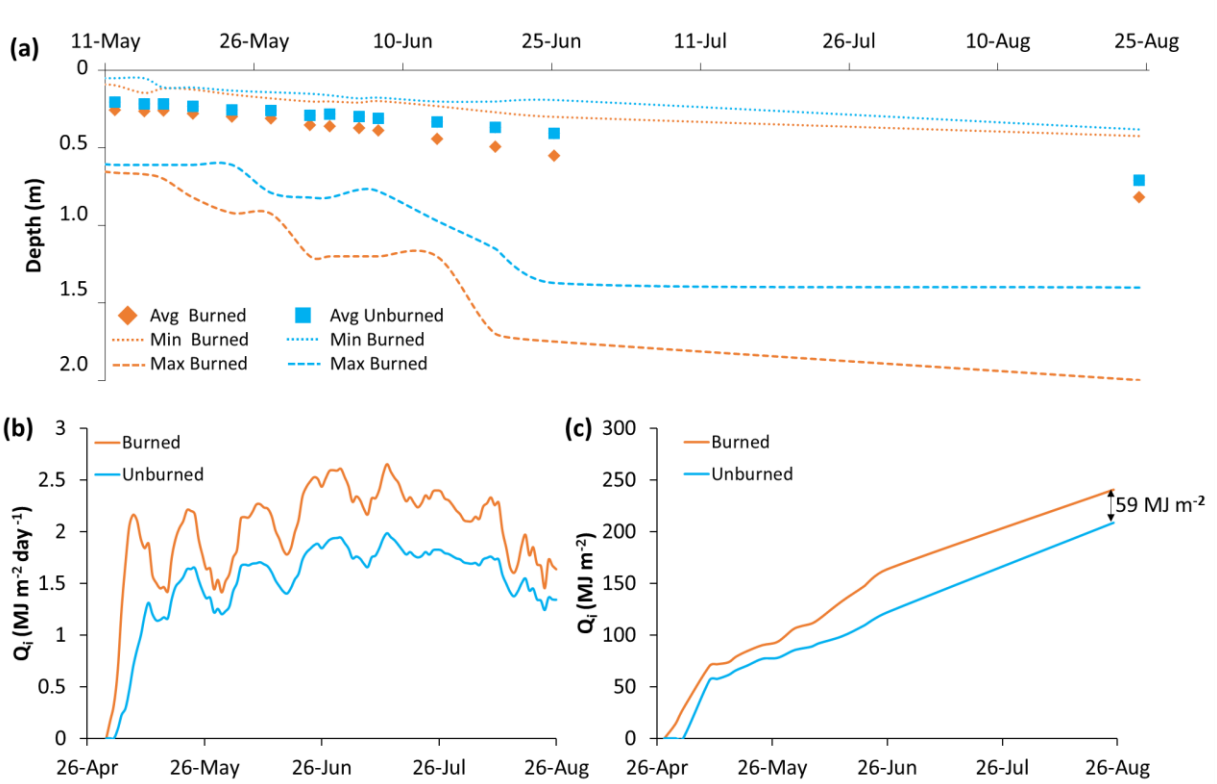

Figure 9. May to September 2015 burned (orange) and unburned (blue) peat plateau (a) frost table (FT) depths, (b) daily and (c) cumulative energy of latent heat used to melt ice (Q_i). Panel (a) shows the average measured (points) FT depths as well as the minimum (dotted) and maximum (dashed) measured FT depths. End of August 2015 average FT depths are deeper on the burned plateau (0.82 m) than the unburned plateau (0.71 m), due to the earlier and greater input of Q_i to the burned plateau (3rd May: 28.7 MJ m^{-2}), and the greater Q_i cumulatively available to the burned plateau (236.5 MJ m^{-2}) than the unburned plateau (177.8 MJ m^{-2}).

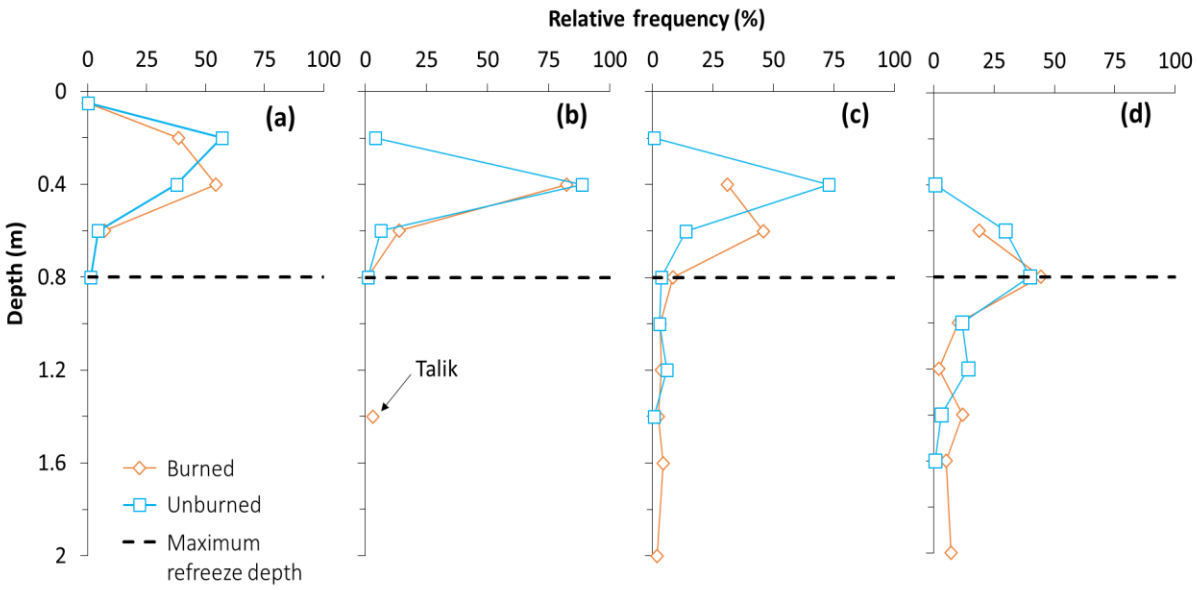

Figure 10. Relative frequency distribution of measured 2015 ground thaw depths along the transect from (a) early (11 May) to (b) late (03 June) spring and (c) early (25 June) to (d) late (26 August) summer on a burned (orange) and unburned (blue) forested peat plateau. The dashed horizontal line at 0.8 m represents the maximum possible overwinter refreeze depth at Scotty Creek, NWT (Connon *et al*., 2018).

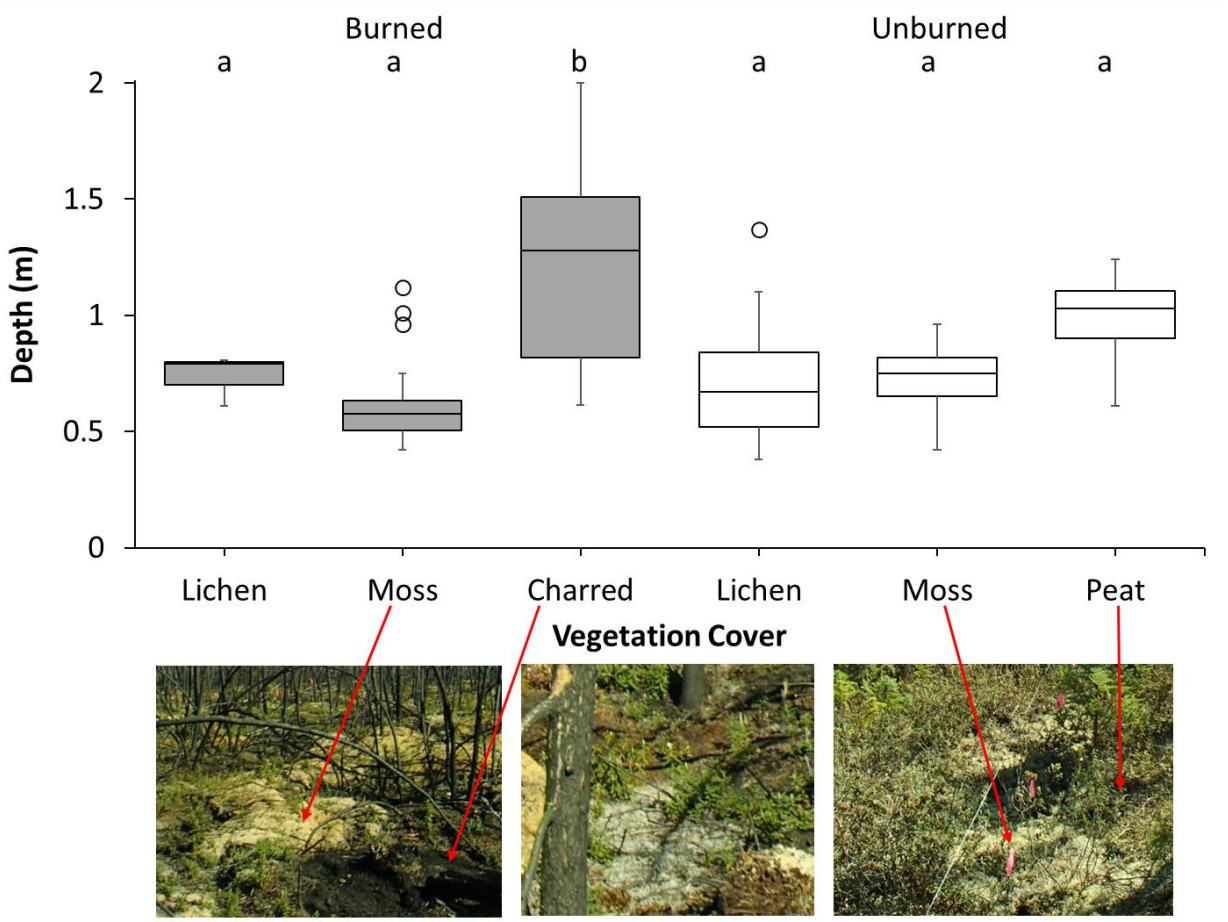

Figure 11. Ground thaw depths on a burned (left; grey) and unburned (right; white) plateau subdivided by the ground cover vegetation at individual measurement points, overlaying the peat. Ground cover types are as follows: Lichens, Moss (*Sphagnum* sp.), Peat covered by Labrador tea on the unburned plateau, and charred peat on the burned plateau.

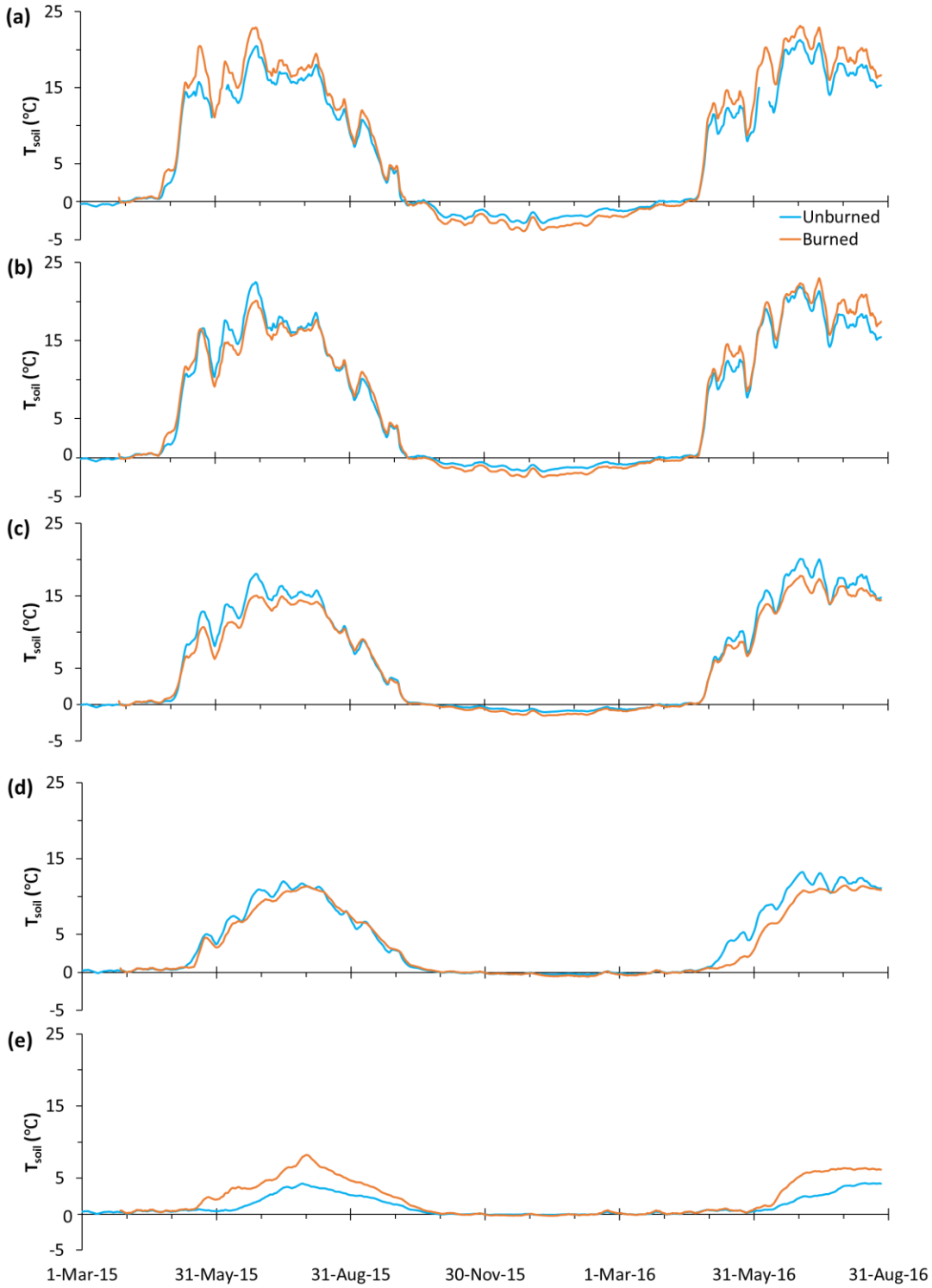

Figure 12. Comparison of burned (orange) and unburned (blue) soil temperatures at 0 cm (a), 8 cm (b), 16 cm (c), 32 cm (d), and 64 cm (e). Overwinter 2015-2016 soil temperatures are significantly warmer on the unburned plateau than the burned plateau at all depths, with exception of 64cm where the burned plateau is warmest in winter due to the release of heat from storage lower in the profile.

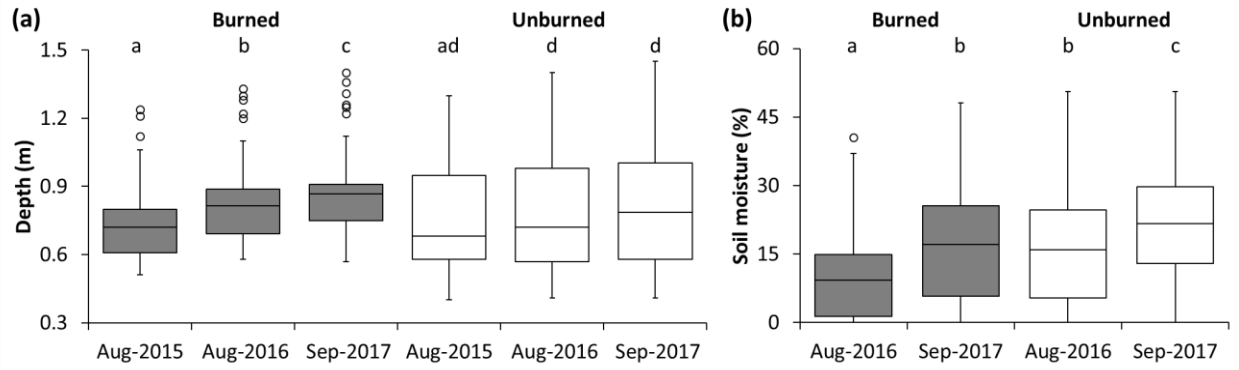

Figure 13. End of the thawing season 3 years post-fire (2015-2017) grid measurements (n=100) of the (a) frost table (FT) depths (m) and (b) 20 cm integrated soil moisture (%) on the burned (grey) and unburned (white) portions of the forested peat plateau. Mean FT depths we're not significantly different between the burned and unburned plateau in 2015, as well on the unburned plateau all three years' post-fire (0.68, 0.72, 0.79 m). Mean FT depths on the burned plateau increased significantly three years post-fire (0.72, 0.82, 0.87 m). Average soil moisture we're significantly drier on the burned plateau (7%, 17%) than the unburned plateau (14%, 23%), in 2016 and 2017 respectively.

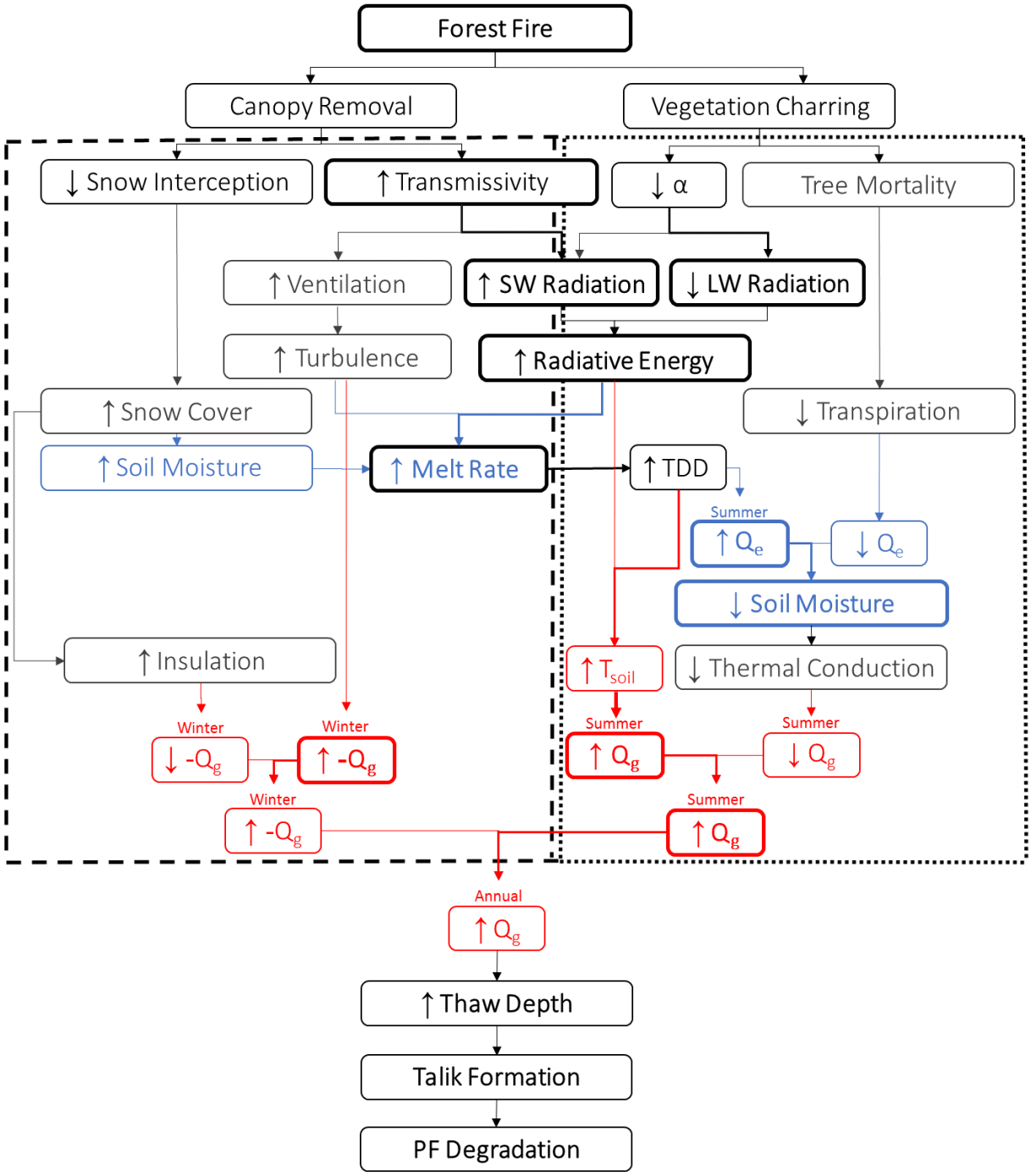

Figure 14. Conceptual model of the components to winter (dashed) and summer (dotted) permafrost (PF) energetics post-fire. Including processes relating to soil moisture and the latent heat flux (Q_e; blue) and processes relating to the ground heat flux (Q_g; red), where α is the ground surface albedo affecting shortwave (SW) and longwave (LW) radiation, and TDD is the thawing degree days, all represented by increases (↑) or decreases (↓). Significantly important processes leading to increased ground heat flux and PF degradation are in bold such as increased radiation, increased melt rate and decreased summer soil moisture.

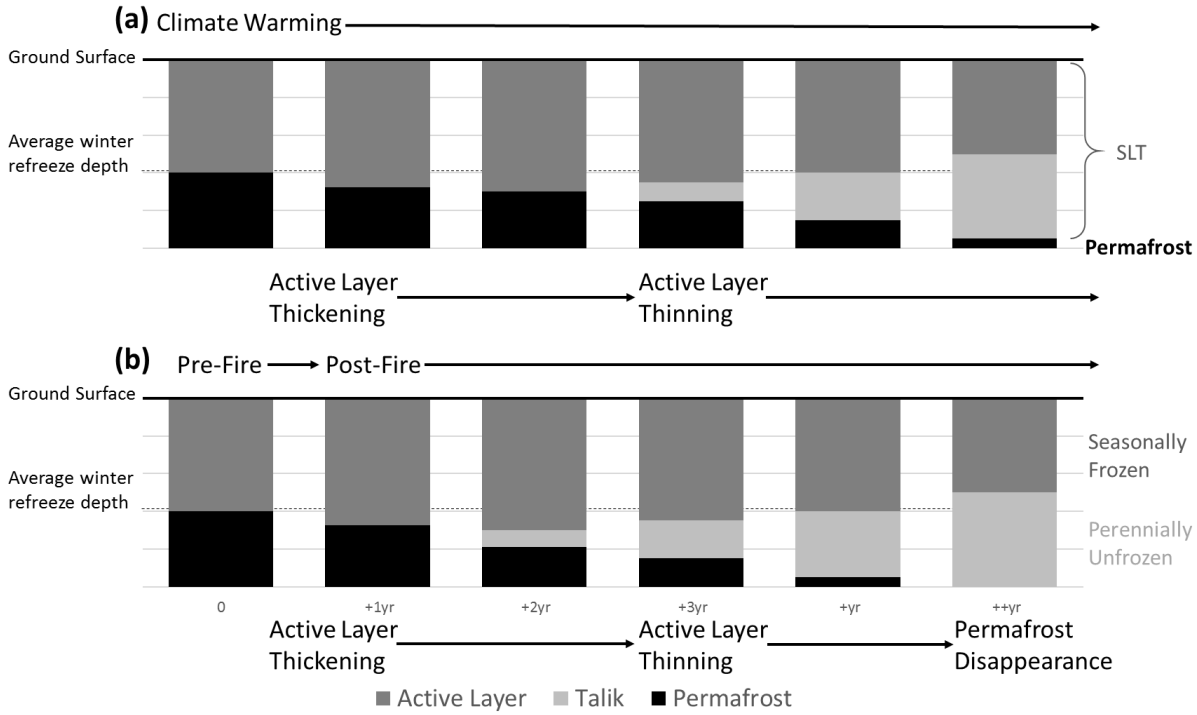

Figure 15. Conceptual diagram of the frozen/unfrozen state of the soil based on field measurements (modified from Connon *et al.*, 2018) due to (a) climate warming on an unburned peat plateau and (b) to forest fire disturbance. Demonstrating talik development through yearly progressive changes to the active layer and suprapermafrost layer thickening (SLT) with climate warming processes on an unburned plateau (a) and accelerated as well as accentuated on a burned plateau (b) due to a low-severity fire. Fires in the study region lead to complete permafrost degradation, remaining in the soil profile is a distinction between seasonally frozen and perennially unfrozen ground regulated by the overwinter refreeze depths (dashed).

CHAPTER 3

3 – CONCLUSION

Previous studies have shown the effects of wildfires on snowmelt (Boon, 2009; Burles and Boon, 2011; Winkler, 2011), and the potential effects on ground thaw (Brown *et al.*, 2015; Liu *et al.*, 2014; Zhang *et al.*, 2015). However, the effects of snowmelt on the subsequent ground thaw post-fire leading to talik development and permafrost degradation remains unquantified. Understanding these processes in remote northern areas is important as the landscape will be further modified with future climatic changes. Furthermore, the importance of considering burned areas when modeling snowmelt and ground freeze/thaw is imperative as burned areas, even those of low-severity, demonstrate different characteristics than the surrounding landscape and as such should be considered as a distinct hydrological response unit with forest fire frequencies expected to increase under future climate scenarios.

3.1 – Principal Findings

End of winter snowpack conditions were significantly different between the burned and unburned portions of the peat plateau. The burned plateau snowpack on average had a greater depth as well as density accounting for a greater snow water equivalent (SWE). Removal of the canopy by fire not only increased the amount of snow on the ground surface but increased the incoming solar radiation reaching the snowpack. Incoming solar radiation is the greatest component to the energy available for snowmelt. With increased energy available for snowmelt, the burned plateau snowpack melted at a faster rate and became snow free earlier.

There was no indication by soil temperatures that an increased depth of the snowpack had a significant insulating effect on ground surface reducing overwinter refreeze depths. Overwinter soil temperatures at various depths were colder than the unburned plateau despite the greater average snowpack depth. As such, depth of the snowpack had no direct effect on increased thaw depths observed post-fire.

Changes to the forest canopy structure by the wildfire affected the ground surface and subsurface temperatures, leading to energy available to melt the ground ice, in the form of latent heat, within the burned plateau. Thaw depth increased at a greater rate on the burned portion of the plateau than the unburned post-snowmelt. End-of-season thaw depths (*i.e.* the suprapermafrost layer) were significantly deeper and become progressively deeper each subsequent year post-fire. Assuming no changes to overwinter refreeze depths, active layer thickness decreases with the formation of taliks. As the active layer is bounded by a permanent thawing front at its base, as such, the suprapermafrost layer increases. Conductive energy from the thawed saturated layer comprising the talik thaws the permafrost below and reduces the depth of overwinter freezeback, which further increases the thickness of the talik.

This study documented the effects of a low-severity wildfire on snowmelt and seasonal ground thaw. A low-severity burn can increase snowfall accumulation as well as the rate and length of snowmelt leading to an increase in ground thaw depth and potential talik formation. The loss of the forest canopy resulted in an increase in solar radiation, increasing the energy available for snowmelt and ground thawing. The rate of snowmelt on the burned portion was greater than the unburned portion of the peat plateau leading to a shortened snowmelt period. Frost table depths at the end of August were significantly deeper on the burned plateau than the unburned, and increased the suprapermafrost layer annually post-fire.

3.2 – Future Work

The conceptual model of this thesis, outlining winter snowmelt and summer ground thaw processes, is the first step in the identification of potential characteristics distinctive to burned landscapes. A better quantification of these characteristics, based on future research, will contribute to more informed parameterization of numerical models of physical processes at larger scales for hydrological modelling.

A potential parameter requiring further quantification includes the overwinter refreeze depth. Average and maximum refreeze depths previously measured at Scotty Creek (Connon *et al.,* 2018) were used during this research based on the assumption that the forest fire had no significant effect on overwinter refreeze depths. However, this may not be the case when talik development is accelerated by the increased ground thaw following a wildfire. Further research building on that by Connon *et al.* (2018), could provide an insight to the changes brought to the average and maximum refreeze depths with wildfires increasing the snowpack depth overwinter.

This thesis presented the effects of a low-severity wildfire on a peat plateau in a discontinuous permafrost landscape in the southern Northwest Territories for three years following a fire. A multiyear study on the effects of more severe burns, following stand death, re-colonization and vegetation restoration could provide further results than those identified by this research. Further studies could improve large scale energy balance models in both burned and healthy forested peat plateaus within the wetland environment.

REFERENCES

Andreas EL. 2002. Parameterizing scalar transfer over snow and ice: A review. *Journal of Hydrometeorology* **3**(4): 417-432.

Andreadis KM, Storck P, Lettenmaier DP. 2009. Modeling snow accumulation and ablation processes in forested environments. *Water Resources Research* **45**.

Baltzer JL, Veness T, Chasmer LE, Sniderhan AE, Quinton WL. 2014. Forests in thawing permafrost: fragmentation, edge effects, and net forest loss. *Global Change Biology* **58**(247): 824-834.

Beilman DW, Robinson SD. 2003. Peatland permafrost thaw and landform type along a climatic gradient. In *Proceedings of the 8th International Conference on Permafrost*, Phillips M, Springman SM, Arenson LU (eds). Zurich: Balkema; 61-65.

Benscoter BW, Thompson DK, Waddington JM, Flannigan MD, Wotton BM, de Groot WJ, Turetsky MR. 2011. Interactive effects of vegetation, soil moisture and bulk density on depth of burning of thick organic soils. *International Journal of Wildland Fire* **20**(3): 418-429.

Bernhardt EL, Hollingsworth TN, Chapin III FS. 2011. Fire severity mediates climate-driven shifts in understory community composition of black spruce stands of interior Alaska. *Journal of Vegetation Science* **22**(2011): 32-44.

Bernier PY, Swanson RH. 1992. The influence of opening size on snow evaporation in the forest of the Alberta foothills. *Canadian Journal of Forest Research* **23**: 239-244.

Boon S. 2009. Snow ablation energy balance in a dead forest stand. *Hydrological Processes* 1-11.

Brown DR, Jorgenson MT, Douglas TA, Romanovsky VE, Kielland K, Hiemstra C, Euskirchen ES, Ruess RW. 2015. Interactive effects of wildfire and climate on permafrost degradation in Alskan lowland forests. *Journal of Geophysical Research: Biogeosciences* **120**: 1619-1637.

Brown RJE. 1983. The Role of Fire in Northern Circumpolar Ecosystems. *Chapter 6: Effects of fire on the permafrost ground thermal regime*. Wein RW, MacLean DA (eds). 97-110.

Burles K. 2010. Snowmelt energy balance on a burned forest stand, Crowsnest Pass, Alberta. (Master's Thesis). University of Lethbridge, Lethbridge, Alberta.

Burles K, Boon S. 2011. Snowmelt energy balance in a burned forest plot, Crowsnest Pass, Alberta, Canada. *Hydrological Processes* 25(19): 3012-3029.

Chambers SD, Beringer J, Randerson JT, Chapin III FS. 2005. Fire effects on net radiation and energy partioning: Contrasting responses of tundra and boreal forest ecosystems. *Journal of Geophysical Research* **110**: D09106.

Chasmer L, Hopkinson C. 2016. Threshold loss of discontinuous permafrost and landscape evolution. *Global Change Biology* **23**(7): 1365-2486.

Chasmer L, Hopkinson C, Quinton W. 2011. Quantifying errors in permafrost plateau change from optical data, Northwest Territories, Canada: 1947-2008. *Candian Journal of Remote Sensing* **36**(2): S211-S223.

Connon RF, Quinton WL, Devoie E, Hayashi M. 2018. The influence of shallow taliks on permafrost thaw and active layer thickness in subarctic Canada. *Journal of Geophysical Research: Earth Surface* **123.**

de la Casinière AC. 1974. Heat exchange over a melting snow surface. *Journal of Glaciology* **13**(9): 55-72.

Dingman SL. 2002. Physical Hydrology, 2nd Edition. *Chapter 5: snow and snowmelt.* Upper Saddle River: Prentice Hall. 159-209.

Environment and Climate Change Canada (ECCC). 2017. Canadian Climate Normals 1981-2010. *Station Data (Fort Simpson A)*. Retrieved from http://cliamte.weather.gc.ca/climate_normals/

Farouki OT. 1981. The thermal properties of soils in cold regions. *Cold Regions Science and Technology* **5**(1): 67-75.

Fedorov AN, Iwahana G, Konstantinov PY, Machimura T, Argunov RN, Efremov PV, Lopez LMC, Takakai F. 2017. Variability of permafrost and landscape conditions following clear cutting of larch forest in cental Yakutia. *Permafrost and Periglacial Processes* **28**(1): 331-338.

Flannigan MD, Logan K, Amiro BD, Skinner WR, Stocks BJ. 2005. Future area burned in Canada. *Climatic Change* **72**: 1-16.

Flannigan MD, Cantin AS, de Groot WJ, Wotton M, Newbery A, Gowman LM. 2013. FGlobal wildland fire season severity in the 21st century. *Forest Ecology and Management* **294**: 54-61.

Gray DM, Prowse TD. 1993. Snow and floating ice. In *Handbook of Hydrology*, Maidment DR (eds). McGraw-hill Inc, New York, NY. (7.1-7.58pp).

Haughton E. 2018. Permafrost thaw-induced forest to wetland conversion: potential impacts on snowmelt and basin runoff in northwestern Canada. (Master's Thesis). Wilfrid Laurier University, Waterloo, Ontario.

Hayashi M, Goeller N, Quinton WL, Wright N. 2007. A simple heat-conduction method for simulating the frost-table depth in hydrological models. *Hydrological Processes* **21**(19): 2610-2622.

Helbig M, Pappas C, Sonnentag O. 2016. Permafrost thaw and wildfire: Equally important drivers of boreal tree cover changes in the Taiga Plains, Canada. *Geophysical Research Letters* **43**(4): 1598-1606.

IPCC (Intergovernmental Panel on Climate Change). 2014. Climate Change 2014: Synthesis Report. *Contribution of working groups I, II, and III to the Fifth Assessment Report of the IPCC,* Pachauri RK, Maeyer LA (eds). Geneva, Switzerland. (151 pp.).

Jafarov EE, Romanovsky VE, Genet H, McGuire AD, Marchenko SS. 2013. The effects of fire on the thermal stability of permafrost in lowland and upland black spruce forests of interior Alaska in a changing climate. *Environmental Research Letters* **8**(3): 035030.

Ji F, Wu Z, Huang J, Chassignet EP. 2014. Evolution of land surface air temperature trend. *Nature Climate Change* **4**: 462-466.

Jorgenson MT, Romanovsky V, Harden J, Shur Y, O'Donnell J, Schuur EAG, Kanevskiy M, Marchenko S. 2010. Resilience and vulnerability of permafrost to climate change. *Canadian Journal of Forest Research* **40**: 1219-1236.

Jungqvist G, Oni SK, Teutschbein C, Futter MN. 2014. Effects of climate change on soil temperatures in Swedish boreal forests. *PLoS ONE* **9**(4): e93957.

Kasischke ES, Christensen Jr NL, Stocks BJ. 1995. Fire, global warming, and the carbon balance of boreal forests. *Ecological Applications* **5**: 437-451.

Kasischke ES, Bourgeau-Chavez LL, Johnstone JF. 2007. Assessing spatial and temporal variations in surface soil moisture in fire-disturbed black spruce forests in Interior Alaska using spaceborne synthetic aperture radar imagery - Implications for post-fire tree recruitment. *Remote Sensing of Environment* **108**: 42-58.

Kopp BJ, Minderlein S, Menzel L. 2014. Soil moisture dynamics in a mountainous headwater area in the discontinuous permafrost zone of Northern Mongolia. *Arctic, Antarctic, and Alpine Research* **46**(2): 459-470.

Kurylyk BL, Hayashi M, Quinton WL, Mackenzie JM, Voss CI. 2016. Influence of vertical and lateral heat transfer on permafrost thaw, peatland landscape transition, and groundwater flow. *Water Resources Research* **52**(2): 1286-1305.

Lau WKM, Kim M-K, Kim K-M, Lee W-S. 2010. Enhanced surface warming and accelerated snowmelt in the Himalayas and Tibetan Plateau induced by absorbing aerosols. *Environmental Research Letters* **5**: 025204. (10pp).

Liu L, Jafarov E, Schaefer KM, Jones BM, Zebker HA, Williams CA, Rogan J, Zhang T. 2014. InSAR detects increase in surface subsidence caused by an Arctic tundra fire. *Geophysical Research Letters* **14**: 3906-3913.

Mackay JR. 1970. Disturbances to the tundra and forest tundra environment of western Arctic. *Canandian Geotechnical Journal* **7**: 420-432.

McClymont AF, Hayashi M, Bentley LR, Christensen BS. 2013. Geophysical imaging and thermal modeling of subsurface morphology and thaw evolution of discontinuous permafrost. *Journal of Geophysical Research: Earth Surface* **118**(3): 1826-1837.

Muller SW. 1947. Permafrost or permanently frozen ground and related engineering problems. J.W. Edwards Inc., Ann Arbor, MI, USA.

Monteith JL. 1957. Dew. *Quarterly Journal of the Royal Meteorological Society* **83**(357): 322-341.

MSC. 2016. National Data Archive of Canada. *Meteorological Service of Canada*. Environment Canada: Dorval, QC, Canada.

National Forestry Database. 2016. Forest fires. *National tables (Table 3.1, Forest fire statistics by province/territory/agency, 1925-2015)*. Retrieved from http://nfdp.ccfm.org/data/compendium/html/comp_31e.html

Neuendorf KKE, Melh JP, Jackson JA. 2005. Glossary of geology Fifth Edition. *American Geological Institute*, Alexandria, Virginia.

Pomeroy JW, Gray DM. 1995. Snowcover accumulation, relocation and management (NHRI Science report No.7) National Hydrology Research Institute, Environment Canada, Saskatoon (144pp).

Pomeroy JW, Schmidt RA. 1993. The use of fractal geometry in modelling intercepted snow accumulation and sublimation. In *50th Eastern Snow Conference*. Québec, QC. (10pp).

Pomeroy JW, Fang X, Ellis C. 2012. Sensitivity of snowmelt hydrology in Marmot Creek, Alberta, to forest cover disturbance. *Hydrological Processes* **26**(12): 1891-1904.

Price AG, Dunne T. 1976. Energy-balance computations of snowmelt in a subarctic area. *Water Resources Research* **12**(4): 686-694.

Quinton WL, Baltzer JL. 2013. The active-layer hydrology of a peat plateau with thawing permafrost, Scotty Creek, Canada. *Hydrogeology Journal* **21**(1): 201-220.

Quinton WL, Baltzer JL. 2013. Changing surface water systems in the discontinuous permafrost zone: implications for stream flow. *Iinternational Association of Hydrological Sciences* **360**: 85-92.

Quinton WL, Hayashi M, Pietroniro A. 2003. Connectivity and storage functions of channel fens and flat bogs in northern basins. *Hydrological Processes* **17**(18): 3665-3684.

R Core Team. 2017. R: A language and environment for statistical computing. Vienna, Austria: R Foundation for Statistical Computing. Retrieved from https://www.R-project.org/

Redding T, Winkler RD, Carlyle-Moses D, Spittlehouse D. 2007. Mayson Lake study examines hydrological processes. *LINK* **9**(2): 10-11.

Rouse WR, Mills PF. 1977. A classification of fire effects on the microclimate of forest and tundra ecosystems: *Final Report, R17-19/2*. Indian and Northern Affaires: Ottawa. (21 pp).

Shur YL, Jorgenson MT. 2007. Patterns of permafrost formation and degradation in relation to climate and ecosystems. *Permafrost and Periglacial Processes* **18**(1): 7-19.

Shur YL, Hinkel KM, Nelson FE. 2005. The transient layer; implications for geocryology and climate-change science. *Permafrost and Periglacial Processes* **16**(1): 5-17.

Skidmore P, Hansen K, Quimby W. 1994. Snow accumulation and ablation under fire-altered lodgepole pine forest canopies. In: *Proceedings, 62nd Western Snow Conference,* Santa Fe, New Mexico; 43-52.

Smith SL, Riseborough DW, Bonnaventure PP. 2015. Eighteen year record of forest fire effects on ground thermal regimes and permafrost in the central Mackenzie Valley, NWT, Canada. *Permafrost and Periglacial Processes*.

Soja AJ, Tchebakova NM, French NHF, Flannigan MD, Shugart HH, Stocks BJ, Sukhinin AI, Parfenova EI, Chapin III FS, Stackhouse Jr PW. 2006. Climate-induced boreal forest change: predictions versus current observations. *Global and Planetary Change* **56**: 274-296.

Spittlehouse DL. 2008. Annual water balance of forest and burnt stands. In *Watershed response to the McLure forest fire*, Moore RD, Winkler RD, Carlyle-Moses D, Spittlehouse DL, Giles T *et al.* (eds). *Streamline* **12**(1): 1-8

Stenberg P, DeLucia EH, Schoette AW, Smolander H. 1995. Photosynthetic light capture and processing from cell to canopy. In *Resource Physiology of Conifers*, Smith WK, Hinckley TM (eds). Elsevier, New Work. 3-38.

Stocks BJ, Mason JA, Todd JB, Bosh EM, Wotton BM, Amiro BD, Flannigan MD, Hirsh KG, Logan KA, Martell DL, Skinner WR. 2003. Large forest fires in Canada, 1959-1997. *Journal of Geophysical Research* **108**(D1): 8149

Vitt, DH, Halsey LA, Zoltai SC. 2000. The changing landscape of Canada's western boreal forest: the current dynamics of permafrost. *Canadian Journal of Forest Research* **30**: 283-287.

Vincent L, Zhang X, Brown R, Feng Y, Mekis E, Milewska E, Wan H, Wang X. 2015. Observed trends in Canada's climate and influence of low-frequency variability. *Journal of Climate,* **28**: 4545-4560.

Wang X, Thompson DK, Marshall GA, Tymstra C, Carr R, Flannigan MD. 2015. Increasing frequency of extreme fire weather in Canada with climate change. *Climatic Change* **130**(4): 573-586.

Williams TJ, Quinton WL. 2013. Modelling incoming radiation on a linear disturbance and its impact on ground thermal regime in discontinuous permafrost. *Hydrological Processes* **27**: 1854-1865.

Williams TJ, Quinton WL, Baltzer JL. 2013. Linear disturbances on discontinuous permafrost: implications for thaw-induced changes to land cover and drainage patterns. *Environmental Research Letters* **8**(2): 025006 (12pp).

Williams TJ, Pomeroy JW, Janowicz JR, Carey SK, Rasouli K, Quinton WL. 2015. A radiative-conductive-convective approach to calculate thaw season ground surface temperatures for modelling frost table dynamics. *Hydrological Processes* **29**: 3954-3965.

Winkler RD. 2011. Changes in snow accumulation and ablation after a fire in south-central British Columbia. *Streamline Watershed Management Bulletin* **14**(2): 1-7.

Winkler RD, Moore RD, Redding TE, Spittlehouse D, Smerdon B, Carlyle-Moses DL. 2010. The effects of disturbance on hydrologic processes and watershed response. In *Compendium of forest hydrology and geomorphology in British Columbia*, Pike RG, Redding TE, Moore RD, Winker RD, Bladon KD (eds). *Land management Handbook* **66**(1): 179-212.

Woo M-K. Permafrost Hydrology. 2012. Springer Science & Business Media: New York. (564 pp).

Woods SW, Ahl R, Sappington J, McCaughey W. 2006. Snow accumulation in thinned lodgepole pine stands, Montana, USA. *Forest Ecology and Management* **235**: 202-211.

Wotton BM, Nock CA, Flannigan MD. 2010. Forest fire occurrence and climate change in Canada. *International Journal of Wildland Fire* **19**: 253-271.

Wright N, Hayashi M, Quinton WL. 2009. Spatial and temporal variations in active layer thawing and their implication on runoff generation in peat-covered permafrost terrain. *Water Resources Research* **45**(5): 1-13.

Yoshikawa K, Botlon WR, Romanovsky VE, Fukuda M, Hinzman LD. 2002. Impacts of wildfire on the permafrost in the boreal forests of Interior Alaska. *Journal of Geophysical Research* **108**(D1): 8148.

Zhang Y, Wolfe SA, Morse PD, Olthof I, Fraser RH. 2015. Spatiotemporal impacts of wildfire and climate warming on permafrost across a subarctic region, Canada. *Journal of Geophysical Research: Earth Surface* **120**(11): 2338-2356.

SUPPLEMENTAL MATERIALS

Details on Snowmelt Energy Balance Parameters

Snow surface energy balance was computed using a one-dimensional energy balance equation with data from the burned and unburned micrometeorological stations and field surveys, those including the following measurements:

K*	Net shortwave radiation (W m^{-2})
L*	Net longwave radiation (W m^{-2})
T_a	Ambiant air temperature (°C)
T_{ss}	Snow surface temperature (°C)
T_s	Internal temperature of the snowpack (°C)
e_a	Atmospheric vapour pressure (kPa)
e_{ss}	Snow surface vapour pressure (kPa)
μ	Windspeed (m s^{-1})
z_a	Height of the wind measurement (m)
SWE	Snow water equivalent (mm)

The following coefficients were used:

λ_v	Latent heat of vapourization	2.48 x 10^6 J kg^{-1}
T_m	Melting temperature of ice	0°C
ρ_w	Density of water	1000 kg m^{-3}
c_i	Heat capacity of ice	2102 J kg^{-1} K^{-1}
k	von Karman's constant	0.4
z_o	Surface roughness coefficient	0.0006 m
g	Gravitational acceleration	9.6 m s^{-1}

Details on Snowmelt Energy Balance Equations

The **energy available for snowmelt**, Q_m (MJ m^{-2} day^{-1}), is computed using a one-dimensional energy balance equation defined as:

$$Q_m = K^* + L^* + Q_e + Q_h + Q_g + Q_r - Q_{cc} \quad (1)$$

Q_m is the sum of the net shortwave (K^*) and longwave (L^*) radiation; Q_e, Q_h, and Q_g are respectively the latent, sensible and ground heat flux, Q_{cc} is the cold content and Q_r the energy input from rain. Q_r was omitted in this study given the lack of rainfall events during the snowmelt period. The ground heat flux (Q_g) is estimated from soil temperatures and moisture data (Gray and Prowse, 1993), Q_g was found to be negligible at the study site (Haughton, 2018).

ASSUMPTION 1: When the snow surface is melting, the overlying air mass temperature is assumed to be 0°C (Price and Dunne, 1976) and a saturated vapour pressure of 6.11 mb (Heron and Woo, 1978).

The **cold content** (Q_{cc}) is the change of internal energy in the snowpack (Gray and Prowse, 1993).

$$Q_{cc} = -c_i * \rho_w * SWE * (T_s - T_m) \quad (2)$$

Where c_i is the heat capacity of ice, ρ_w is the density of water, T_s and T_m are the average temperature of the snowpack and melting point of ice. The snow water equivalent (m) is calculated as the product of the snowpack density and depth.

ASSUMPTION 2: The Q_{cc} is included as large changes in internal energy can occur within shallow snowpacks when it melts during the day yet freezes overnight, whereas most studies consider the Q_{cc} negligible as the T_s during snowmelt is near or at 0°C.

Heat fluxes

The **sensible heat flux** (Q_h) is calculated as a function of the temperature gradient, *i.e.* the difference in the snow surface and the overlying air mass:

$$Q_h = \rho_a * C_{\rho a} * D_h * (T_a - T_{ss}) \quad (4)$$

where ρ_a is the density of air (kg m^{-3}), $C_{\rho a}$ is the heat capacity of air at a constant pressure (J kg^{-1} K^{-1}), D_h is the bulk sensible heat transfer coefficient (m s^{-1}), and T_a and T_{ss} are the temperatures of the air and snow surface (K).

The **latent heat flux** (Q_e) is calculated as a function of the vapor gradient, *i.e.* the difference in the snow surface and the overlying air mass:

$$Q_e = \rho_a * \lambda_v * D_e * \frac{0.622}{P} * (e_a - e_{ss}) \quad (5)$$

where λ_v is the latent heat of vapourization, D_e is the bulk latent-heat transfer coefficient (m s^{-1}), P is the atmospheric pressure (kPa), e_a and e_{ss} are atmospheric and snow surface vapour pressures (kPa).

ASSUMPTION 3: Under stable($Ri > 0.3$) and unstable ($Ri < 0.3$) atmospheric conditions, diffusivities of vapour (D_e) and heat (D_h) are corrected following the method of Price and Dunne (1976).

Atmospheric stability

Under neutral atmospheric conditions the bulk transfer coefficient for sensible heat (D_h) equals the bulk transfer coefficient for latent heat (D_h) (Dingman, 2002) and can be derived from the bulk transfer coefficient for momentum (D_M) (Price and Dunne, 1976):

$$D_e = D_h = D_M = \frac{k^2 \mu_a}{\ln(z_a / z_o)} \quad (6)$$

where *k* is the von Karman's constant, μ_a is windspeed (m s^{-1}), z_a is the height of the wind measurement (m), and z_o is the surface roughness (m).

ASSUMPTION 4: Surface roughness coefficient (z_o) is assumed as 0.006 m as it represents the average value between the seasonal and wet snow covers. The horizontal wind speed is assumed as 0 at the snow surface and increases logarithmically to the measurements height above the snow.

The **Richardson bulk stability parameter** (Ri; dimensionless) is used to assess the stable (Ri > 0.3) and unstable (Ri < 0.3) atmospheric conditions (Andreas, 2002):

$$Ri = \frac{g(T_a - T_{ss})}{\mu_a^2 T_a} \quad (7)$$

where g is gravitational acceleration (m s^{-1}), μ_a is windspeed (m s^{-1}), T_a and T_{ss} are the mean air and snow surface temperatures (K).

Correction for stable conditions is:

$$D_{Ms} = {}^{D_M}/_{(1 + 10Ri)} \quad (8)$$

Correction for unstable conditions is:

$$D_{Mu} = D_M * (1 - 10Ri) \quad (9)$$